1-1-2015

Fabrication And Characterization Of A Robust, Field- Deployable, Optical Sensor Designed To Detect Particles In Oils.

Navya Pandreka
Wayne State University,

FABRICATION AND CHARACTERIZATION OF A ROBUST, FIELD-DEPLOYABLE, OPTICAL SENSOR DESIGNED TO DETECT PARTICLES IN OILS.

by

NAVYA PANDREKA

THESIS

Submitted to the Graduate School

of Wayne State University,

Detroit, Michigan

in the partial fulfillment of the requirements

for the degree of

MASTER OF SCIENCE

2015

MAJOR: BIOMEDICAL ENGINEERING

Approved By:

_____

Advisor Date

DEDICATION

To my Father Srinivasa Rao, Mother Kalyani and my Brother Sai Krishna, you guys made it possible with your love and support.

Thank you for everything

ACKNOWLEDGEMENTS

This project would not be possible without the help of many people. I would like to thank my family, friends and my husband for their constant support and encouragement and for keeping me focused.

Time spent at Wayne state university was a great asset to my development. I thank my thesis committee and research advisors, Dr. Gregory Auner, Dr. Rachel kast, Dr. John Cavanaugh, Dr. Michelle Brusatori and Dr. Mahendra Kavdia. Dr. Tara Twomey and Dr. Sally Yurgelevic were really helpful for helping me in growing microbes and teaching equipment's around the lab. Special thanks to Dr. Auner and Dr. Kast for helping me in designing the project. I thank David, Barb and Dr. Kiran for their help. I thank all SSIM team for their numerous efforts for making my project successful.

I would like to thank Translume.Inc team for lending their equipment for my project. I thank Dr. Philippe Bado for trusting my ability to work with the equipment and his constant support and I thank Chris for helping me to understand the working mechanism of the equipment. I would like to thank my mentor and friend Dr. Abhishek G, his mentoring all through my master's program was undeniable.

TABLE OF CONTENTS

LIST OF TABLES

LIST OF FIGURES

CHAPTER 1: BACKGROUND AND SIGNIFICANCE

1.1 Fuel Bio deterioration

Biodeterioration of aviation, marine and ground fuels has caused serious economic, safety, and environmental problems [1]. Usually it occurs when water is introduced into the oil by condensation or damage in the infrastructure. Water and oil interface is a favorable environment for microbial growth [1]. Growth of bacteria affects the quality of the fuel and alters other properties such as lubricity. This leads to the wear in the pumps and other friction areas [2].

In 1952, fuel pump failure in some aircraft was observed. This is due to the sulphide corrosion by sulphite reducing bacteria that is found in fuel storage tanks with water droplets [4]. Deterioration of aviation fuel is primarily caused by bacteria and fungi. These include genera Cladosporium, Pseudomonas, Corynebacteria, Candida and Penicillium species among others [4].

The following table shows the frequency of different bacteria and fungi that can be found in aviation fuel [4].

	Aviation fuel		
Microorganisms	**Joint hydrant storage tank (JHST)**	**Aircraft tank (AT)**	**Growth in fuel-mineral salt broth**
Bacillus subtilis	8	10	✓✓✓
Bacillus megaterium	3	6	✓✓
Flavobacterium oderatum	8	8	✓✓
Sarcina flava	4	8	✓✓
Micrococcus varians	6	5	✓✓✓
Pseudomonas aeruginosa	10	10	✓✓✓
Bacillus licheniformis	1	2	✓✓
Bacillus cereus	3	6	✓✓
Bacillus brevis	4	2	✓✓
Candida tropicalis	8	9	✓✓✓
Candida albicans	10	8	✓✓✓
Saccharomyces estuari	4	7	✓✓
Saccharomyces cerevisiae	6	8	✓✓

Schizosacchanomyces pombe	8	7	✓✓✓
Aspergillus flavus	5	8	✓✓✓
Aspergillus niger	3	6	✓
Aspergillus fumigatus	2	3	✓✓✓
Cladosporium resinae	8	9	✓✓✓
Penicillium citrinum	6	7	✓✓
Penicillium frequentans	2	4	✓✓

✓✓✓	Abundant growth
✓✓	Moderate growth
✓	Minimal growth

Table 1: The frequency of different bacteria and fungi that can be found in aviation fuel

Nine different bacteria and fungi show abundant growth in fuel systems from the above data. This project mainly concentrate on one bacterium and its detection utilizing femtosecond laser micro machined microfluidics device [4].

1.2 Pseudomonas aeruginosa

Pseudomonas aeruginosa is a gram-negative bacterium that can adapt to the harsh environment of fuel due to its metabolism versatility. A wide range of hydrocarbons can be degraded by P. aeruginosa as it grows in jet fuel storage systems. It is proposed that P. aeruginosa is important for bioremediation of light non-aqueous phase liquids. These alkanes act

as sole carbon source for these bacteria. Alkanes in the fuel are metabolized via oxidation process and this is done with a genome of P.aeruginosa that contains the two membrane bound alkane hydroxylases and essential electron transfer proteins, rubredoxins and FAD-dependent NAD(P)H2 rubredoxin reductases [5].

Figure 1: Pseudomonas aeruginosa

Picture courtesy: Pseudomonas Genome Database publication. Used with permission

1.3 Cladosporium resinae

Cladosporium resinae or Hormoconis resinae became famous with the name "Kerosene fungus". This fungus reportedly found around in 1960's in aircraft fuel tanks but it was not confirmed due to the existence of other microbial growth in the fuel tanks [6]. This appeared to be worldwide problem with sample rates as high as 78% of all fuel samples from Australia contains C. resinae and 80% of fuel samples in America [6].

C. resinae strains grow on C9 to C18 n-alkanes but limited growth is observed on C10, C14, C16 and no growth on C12. It is one of the fungi that is widely spread in both rich hydrocarbons and poor hydrocarbons environment and is a potential cause of fuel degradation [7].

Figure 2: Cladosporium resinae

"Photograph: Keith A. Seifert, copyright Her Majesty the Queen in Right of Canada as represented by the Minister of Agriculture and Agri-Food. Used with permission. "

It is also evident that C. resinae doesn't compete with other organisms and absence of organic nitrogen and pesticides presence wont effect C. resinae and can proliferate the ecological niches [7].

1.4 Zirconium oxide beads

Zirconium is a unique material, and it is one of the dense forms of ceramic. These Zirbeads have uniform size and shape and hard material. They are non-porous and extreme smooth. They exhibit high mechanical resistance to chipping and fractures. They are even resistant to all acids and alkali and they are non-conductive and non-magnetic [9].

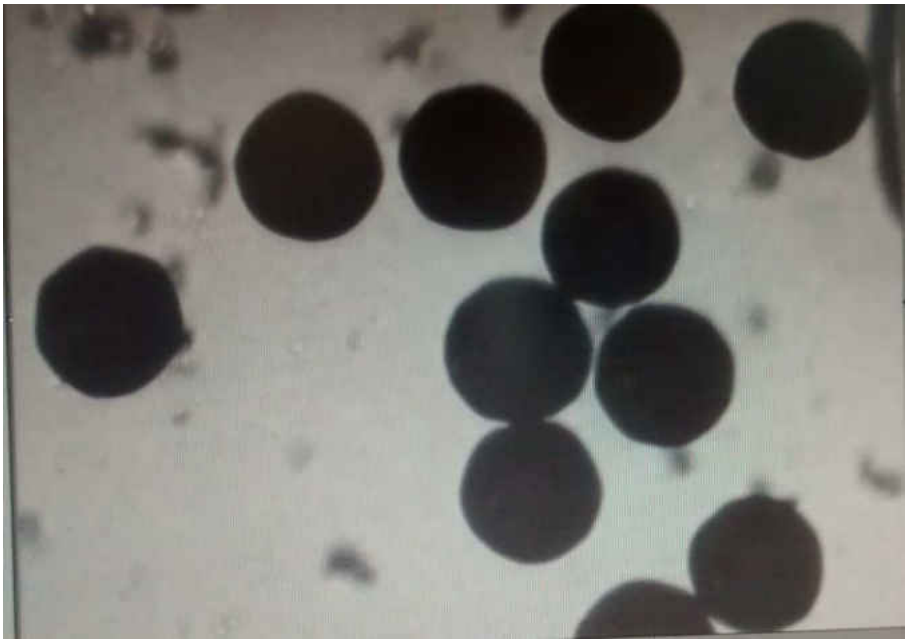

Figure 3: Zirconium oxide beads under microscope 10x,

Reference: Translume.Inc. Used with permission

1.5 Specific Aim

The main aim of this project is to develop a sensor that can detect bacteria and other ferrous and non-ferrous debris that are present in the aviation fuel. This sensor will have a real time capability to detect lubricant contaminants and bearing degradation as well as biological contamination. Here optical techniques are used to detect these particulates. This sensor will feature a robust optical system that is an integral part of the body of the sensor. This hybrid system is uniquely suited to operate in environments where high levels of vibrations and shocks are present.

CHAPTERS 2: GLASS MICROFLUIDICS

This chapter deals with glass microfluidics and femtosecond laser, followed by methods involved in the fabrication of a glass chip.

2.1 Glass Microfluidics

The glass microfluidics sensors used in this project are Lab on chip (LOC) devices and provides fluidic analysis with less sample volumes, down to less than Pico liters. These are manufactured using femtosecond laser pulses as it has the property of changing the refractive index of fused silica [3]. Fused silica and quartz materials had been used in manufacturing of glass microfluidics. This method can be used to create miniaturized devices that are useful in the micro and nano-systems. The traditional method relies on two main technologies, a) clean room process b) conventional microfabrication processes [3].

2.2 Microsystems fabricated using femtosecond lasers

Ultra high peak power pulses produced from femtosecond laser t are different from the conventional long-pulse lasers. Multiphoton processes were observed in femtosecond laser. It gives the new opportunity to tailor the miniaturized devices, and it provides excellent spatial resolution and can be utilized to fabricate three- dimension structures [3]. Even though peak power is enormous in GW/mm2, the average power is small. The average power used in these devices would be 200-mW.The effect of femtosecond laser on dielectric materials is still unclear [3].

The glass typically used for this is synthetic amorphous silica (a-sio2), and it has outstanding optical properties and is inert to most chemicals. Apart from this quality, fused silica has excellent elastic properties that make more flexible for microsystems, and the raw material to make fused silica it is the most abundant material on the planet [3].

When fused silica is exposed to the femtosecond laser, three different regimes are observed.

- In first energy threshold E1, the material refractive index and etching susceptibility are locally increased. However, some of these phenomenons are still in the debate [3].
- In the second energy threshold E2, the formations of self-organized patterns are observed by our research and others [3].
- Further, if the energy density increases, formation of voids is observed in the silica [3]. And this is the main mechanism for selective etching by HF.

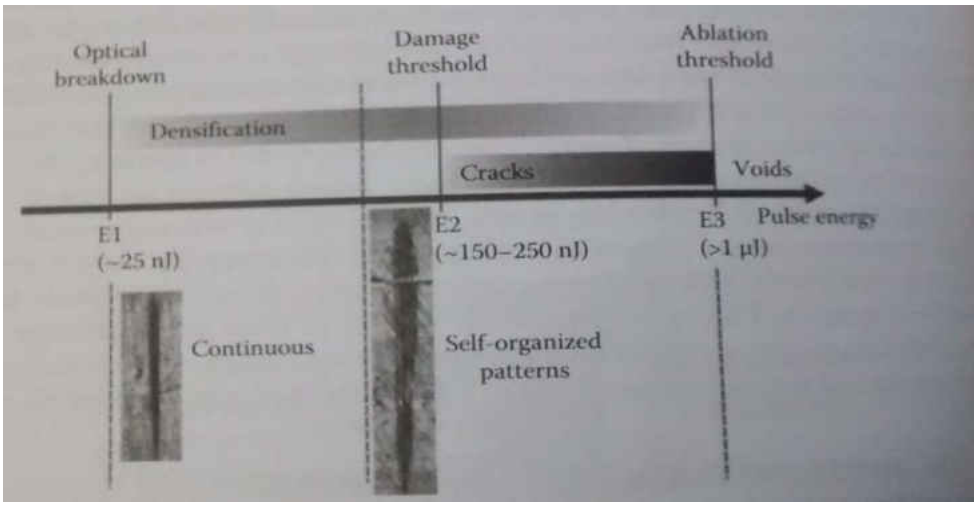

Figure 4: Effect on fused silica for different pulse energies.

Picture courtesy: Optical Nano and Micro Actuator Technology.Page-474

2.3 FemtoWrite ™ and FemtoEtch ™

For a long time it is know that doped glass index of refraction can be changed with exposure to light. Silica fibers were photosensitive to UV exposure as discovered by Hill,et Al due to localized damage[8]. This had a major impact on telecommunication devices industry [8]. The major breakthrough came when undoped fused silica, the refractive index was changed by femtosecond pulses and this was discovered by Hirao et. al. [8] He applied this principle to the formation of subsurface waveguides [8].

Later this process was extended by Translume.Inc for the manufacturing of high-quality, low-loss, single mode straight and curved waveguides known as FemtoWrite.

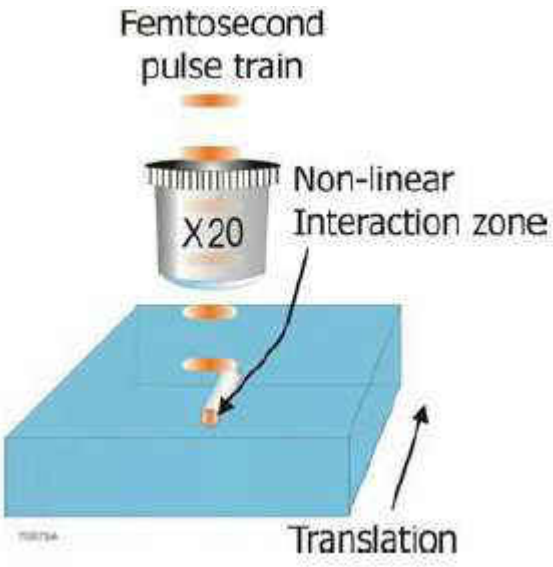

Figure 5: The FemtoWrite

Reference: Translume.Inc Used with permission

The FemtoWrite process is based on the use of femtosecond laser pulses, which are focused inside a fused silica substrate [8]. *"At the focal point, the optical field is so intense that, through multiphoton or tunneling ionization and subsequent impact ionization, an electron plasma is formed"* [8]. The pulse produced from it is short (100fs) and has little energy (1μj) and the glass re-solidifies in a short time compared to the conventional phonon based heat distribution and network vibrations [8]. This was further studied using Raman Spectroscopy. *"Data from Raman Spectroscopy indicated that zones treated with femtosecond laser irradiation contain a distribution of sio2 ring structures weighted toward the smaller member rings when compared to the untreated material."* [8] The formation of smaller size siloxane rings indicated that the zone is densified and have a higher elevated refractive index [8].

One can change the parameters of femtosecond laser pulse and tailor the fused silica local refractive index [8]. This change in refractive index can turn into a waveguide in the glass substrate. The data collected on change in refractive index (delta n < 1%) would look small but it is much more similar to the commercial single mode optical fiber [8].

In the companion femtoEtch process zones treated with femtolaser second laser irradiation are susceptible to hydrofluoric acids (HF) etching [8]. HF will etch away the exposed regions of femtolaser rather preferentially as compared to the unexposed regions. The ratio of etched regions is 100 to 1 [8].

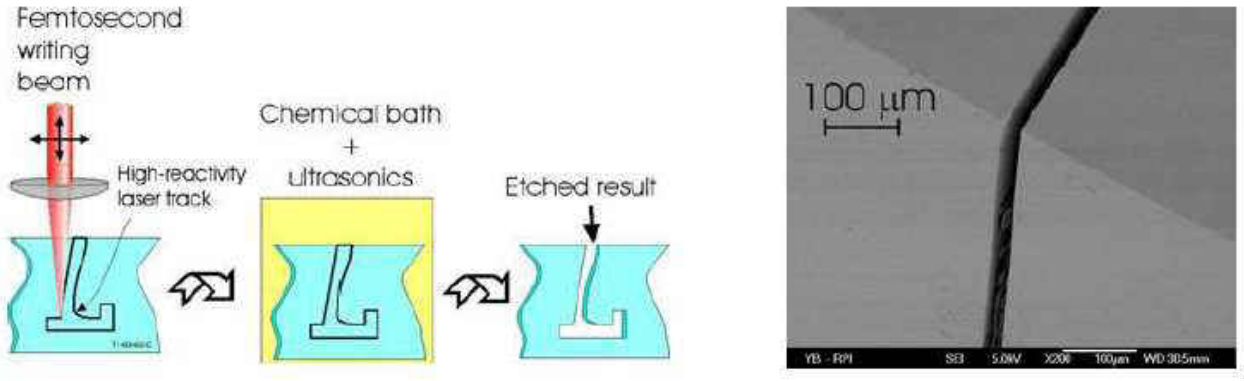

Figure 6: FemtoEtch process

Reference: Translume.Inc Used with permission

The sample is immersed in a hydrofluoric acid bath where the laser exposed tracks are preferentially etched away. This operation results in the formation of a three dimensional glass body of the desired shape. Normally it is difficult to manufacture tunnels, and those tunnels would be a few millimeters long. However, in this scenario one can fabricate high aspect ratio channels that can be covered with a bonded with a fused silica lid [8].

This process is applied to machine mechanical structures, optomechanical elements, and optical elements. In addition, fused silica chips have also developed a high-temperature thermal bonding process, which is used to produce fused silica devices made from multilayers [8].

2.4 Bonding

The cover for the microfluidic channel was formed by another lid of fused silica bound to the micro machined channel substrate. While there are many techniques available, many of them are not directly applicable to binding silica. Most compatible bonding techniques include thermal bonding and optical contact bonding [8].

2.4.1 Optical Contact Bonding

Optical Contact Bonding is a slow process. Here two temperatures are involved in bringing the highly polished glass slides together with the help of Vander Waals attraction. This process is annealed by exposing to relatively low temperatures to create the ionic/covalent bonds. The bonding surfaces have to be in perfect physical contact or else it would end up with a defective bond. The bonding surfaces must have high polished and flat. The cleaned surfaces are made in physical contact only in a clean room. This process is very expensive due to its extreme surface preparation requirement [8].

2.4.2 Thermal Bonding

Thermal bonding is an old process and it is used to fabricate the hollowed mirrors and telescope optics. The fused silica layers are placed in physical contact and bonded in a high temperature furnace. Temperature is increased to the silica softening point (1665^0C) then lowered to 1145^0C, for annealing. Later it is cooled to room temperature. Processing time depends on the glass thickness. Since the temperatures are high, there is possibility of slight deformation of silica but it normally negligible. Temperatures are carefully monitored and controlled to avoid non-uniformity in the bonding [8].

2.5 Manufacturing cost

This process is less expensive compared to flow cytometer techniques that are available in market. However it is good to be pointed out that manufacturing process depends on direct write that generate in serial fashion and it is unlikely to reach low costs. The manufacturing technique is generally production based on photolithographic process [8].

.

CHAPTER -3: DESIGN AND FABRICATION OF MICROCOUNTER

This chapter describes the design and fabrication of the micro-counter optical sensor. Optical sensor detection method and methodologies are discussed further.

3.1 Microcounter

There are a variety of analytical methods to identify the microorganisms that are present in a sample. Utilizing a simple staining method or under fluorescence microscope one can identify some of the microbe or fungi types. When looking in the bigger image, there is a need of personal Micro-counter that can be field deployed. Micro-counters provide much more potential results comparing with the expensive equipment that are not transportable.

The miniaturized Micro-counter benefits are vast. This includes reduction of consumables, smaller foot print, enhanced portability, and integration with networking capabilities, increased robustness and enhanced reliability. Even though there are some manufacturing issues but they are slowed down as the field is advanced. An ideal flow cytometry is always field deployable, low power consumption and light weight. It should be capable of measuring both size and shape of the particle that is passed through it.

3.2 Design and Fabrication of a Micro counter

A standard commercial micro-counter has a couple of essential elements, as illustrated:

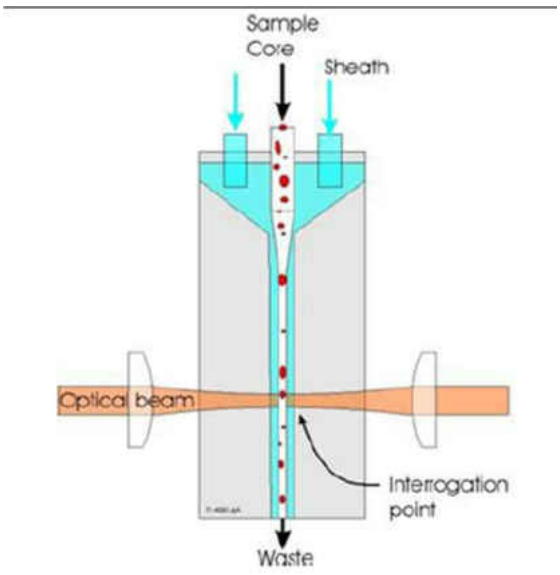

Figure 7: Schematic of generic micro-counter

Reference: Translume.Inc. Used with permission

(a) A microfluidic system which generates a liquid stream formed from a core sample enrobed in a sheath fluid. This fluid flow carries and aligns the objects of interest (in our case the bacteria or non-ferrous debris) so that they pass single-file through the optical system.

(b) A sensing optical system, composed of a minimum of a source, some beam shaping optical elements, and a photodetector to detect the presence of bios, and size them. The bios are commonly detected via scattering and/or fluorescence.

3.2.1 Micro counter Development

For micro counter, it is idolized to use conventional lens-based design. The beam was made elliptical using spherical and elliptical integrated lenses. It was found experimentally that it was better to use a pair of lenses (one spherical and one elliptical) rather than a single aspheric lens. It may be due to the machining capability rather than fundamental optical physics. A major design was the adoption of a vertical geometry of the microfluidic system. (Vertical geometry:

sample flows along the smaller axis of the glass slab, as illustrated in below figure). This micro counter geometry eases the implementation of a higher performance lens-based optical system.

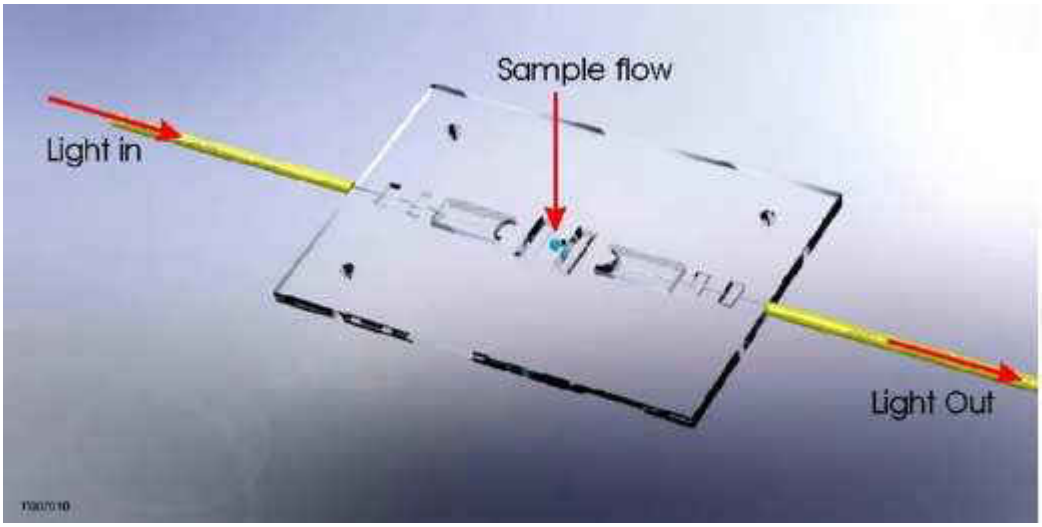

Figure 8: Optical layer with one input and one output fiber. Note the fluid flow propagation direction.

Reference: Translume.Inc. Used with permission

A design was selected where the optical beam is approximately twice as large (1/e2) as the flow channel. Consequently, a significant amount of the optical beam does not sample the microfluidic channel. Optical deflectors are inserted (slots angled to provide total internal reflection) to prevent the majority of this light reaching the detector. Another spherical and cylindrical lens pair is used to focus the optical signal into an outgoing fiber connected to the photodetector.

The input spherical lens collimates the beam (see below figure 9). This defines the beam width, which is, by design, larger than the microfluidic channel. The cylindrical lens reduces the beam height at the level of the microfluidic channel, which is illuminated by a slit shape beam. The height of the interrogating beam is controlled by the radius of curvature of the cylindrical lens (and its relative distance to the microfluidic channel).

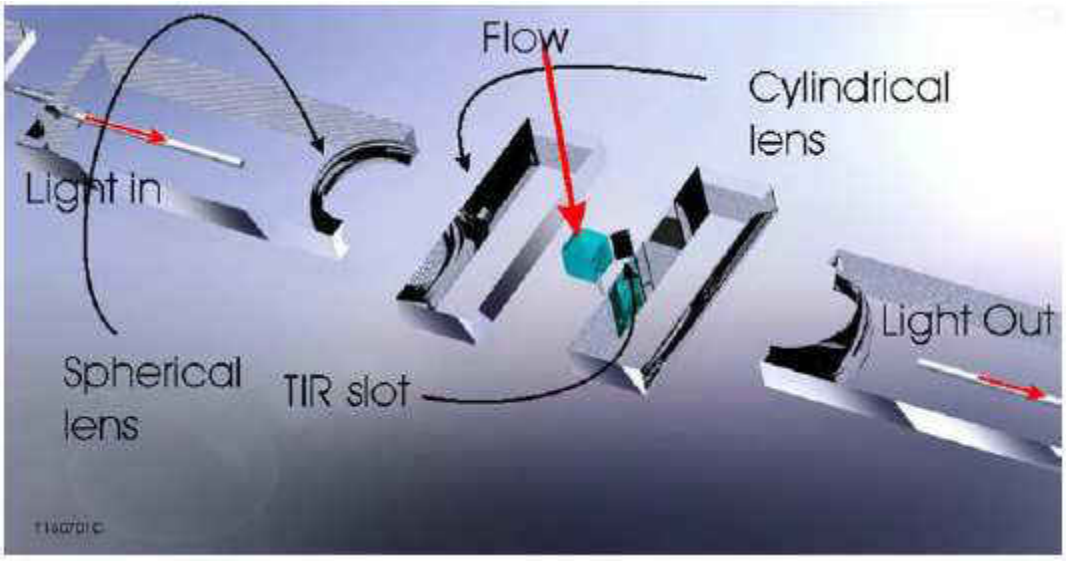

Figure 9: Optical elements integrated in the optical layer (from the left to the right). Input fiber – spherical lens cylindrical lens TI slots (2x) – cylindrical lens – spherical lens output fiber. Reference: Translume.Inc

3.2.2 Chip Construction:

Microcounter is stacked with eight different layers of fused silica that are exposed to the femtosecond laser pulses. The fluid in microcounter flow in vertical direction from top to bottom. This division of functionality was found convenient, especially during the early fabrication and testing rounds.

This method was used as it has a higher chance of detecting a particle that is passing through two optics that are arranged parallel to each other. The distance between these two optics is approximately 3mm. When a particle passes through this system, it will block the light for 0.01 second (on average for the target objects) and the deviation is detecting by the photodetectors that are arranged opposite to the light source.

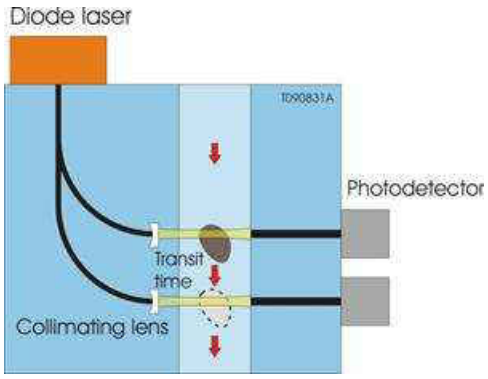

Figure 10: Particle detection through two beams.
Reference: Translume.Inc. Used with permission

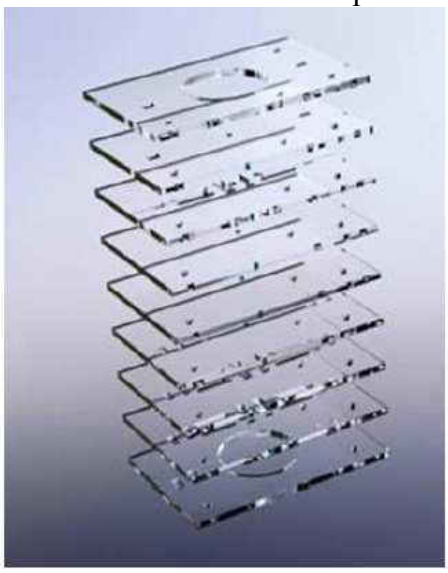

Figure 11: Exploded view of the eight layers forming a unit showed prior to assembly and bonding.
Reference: Translume.Inc. Used with permission

Each layer has its own function. The two layers in the middle are optical layers separated by spacers. There are two position layers, here luers are glued, there is a spacer between positioned layer and optical. It was added as it will give a maximum length and flow rate for the fluid. The channel is a rectangular channel with a width of 300 microns and dimensions of each fused silica layer is 25.4 mm x 33.8 mm, a thickness of 0.50mm for the spacer and position layers, and 1mm for the optical layer.

Thermal bonding was performed to fuse the layers. Here layers 2 to layer 7 are bonded first and layer 1 and layer 8 is bonded layer after. The total weight of chip is 2.37gms.

3.2.3 Fabrication overview

The fabrication of chip and optical system was developed at Translume.Inc. Translume has developed the processes based on the use of femtosecond lasers to precision machine fused silica glass. They use these processes to manufacture microfluidic chips, optical devices, and optical analyzers. They use fused silica (a high quality glass) whose material characteristics are locally modified using femtosecond laser pulses. They have developed two direct write processes to

(a) Change the fused silica index of refraction; And

(b) Change its susceptibility to HF etching. The index of refraction change is used to create optical waveguides within the fused silica substrate (this process is called as *FemtoWrite*^{TM}*)* ;and the second process (*FemtoEtch*^{TM}) is used to shape the fused silica.

3.2.4 Wavelength Selection

Most Micro-counter relies on optical sources that emit in the blue or UV range. These are preferred because they use scattering for detection, and scattering cross sections are much larger at shorter wavelengths. For this device a wavelength of 1550nm was chosen. This choice was motivated by several factors:

1. Commercial micro-counters do not use diode lasers. They mainly use diode pumped solid-state lasers. While the output of these lasers may be delivered using optical fibers, the laser fiber interface is mechanically complex (see below figure) and susceptible to rapid misalignment.

2. Blue diode lasers were not commercially available at the start of this program. One can now purchase diode lasers that operate at 405nm or 445nm. These sources are not commercially

available with fiber pigtail output, even though expected this to change in the not too distant future.

3. Robust 1550nm fiber pigtailed diode lasers (developed for the telecommunication industry) are commercially available, and they are rather inexpensive.

Figure 12: Diode pumped Solid-state lasers

Reference: Translume.inc. Used with permission

4. Micro-optics, fabricated using our femtoEtch™ process (see description below), has rough surfaces which strongly scatter optical beams at short wavelengths. This is a very significant design factor. Test results showed that the signal to noise ratio when operating at short wavelengths (blue / near UV) was too low to allow for the detection of isolated biological objects. This is not because the signal strength is too low, but rather that the relative noise (due to unwanted scattering) is too high.

3.2.5Micro-counter - Flow Cell Testing

This micro counter has the capability to measure fluid velocity through the instrument. This unit was tested using PMMA microspheres (with diameter 5μm, 20μm, and 50μm). The signal to noise ratio was found to be significantly better at 1550nm excitation wavelength.

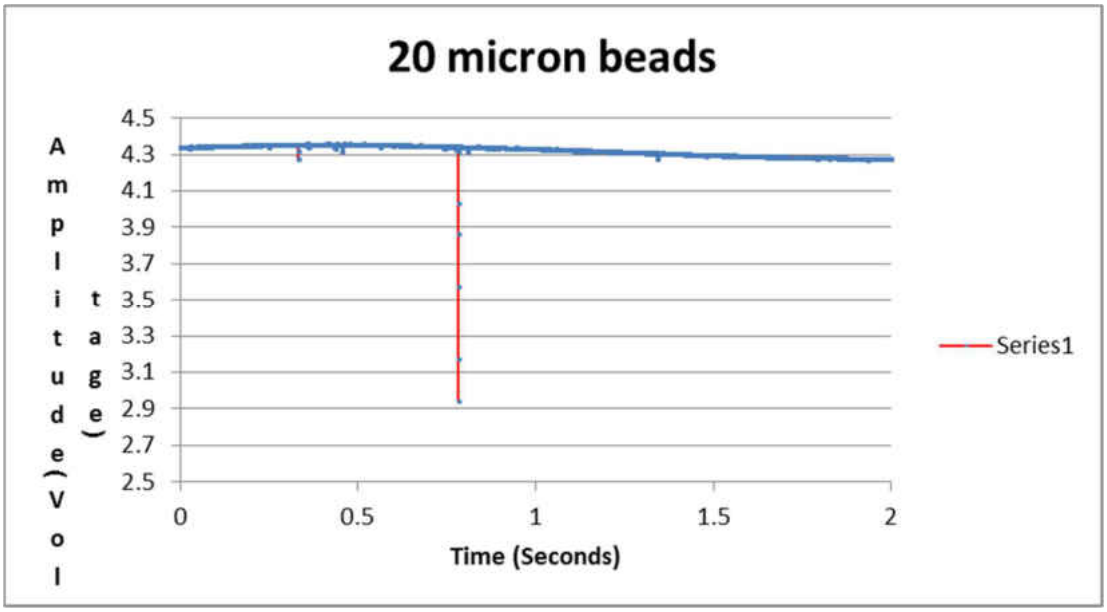

Figure 13: Typical signal to noise (20 micron bead – untreated data)

3.3 Analog Board Design

Translume.Inc. built the Quad PD Dual LD Board (PDLD Board) supports up to four photodiode inputs and up to two laser diode outputs. The board is designed to allow a great deal of flexibility to accommodate a wide variety of photodiode and laser diode devices.

Each photodiode channel is processed to provide a baseline-adjusted voltage signal representative of the photodiode current; an integrated version of the photodiode signal; and a peak-detected version of the photodiode signal. PD #1 is used as the trigger source for processing all of the photodiode channels. The integration period timing is configurable as needed.

Each laser diode channel can operate in constant-current mode or either of two constant-power modes. In constant-current mode, a pot on the board is used to adjust the current going through the laser diode. In integrated-feedback constant-power mode, the laser diode's internal photodiode is fed back to a trans impedance circuit with a pot in the feedback path, allowing the optical power level to be adjusted by the pot based on the feedback from the integrated

photodiode. In independent-feedback constant-power mode, one of the independent photodiode input channels with a pot in the trans impedance amp feedback path is routed to the laser diode control circuitry, allowing the pot to adjust the optical power level of the laser diode based on the independent photodiode feedback.

The detailed description of the board is mentioned in Appendix B.

CHAPTER 4: RESULTS

This chapter discusses the experimental set-up involved in detecting ceramic beads and Pseudomonas aeruginosa and show corresponding results

4.1 Experimental set up

For micro-counter four main parts are required.

- Particle detecting microfluidic chip: Translume MCA866
- Analog board: Translume model 1108171 Rev A, SN 007
- Analog to digital converter: National Instrument Model USB-6009
- Power supply: 4D size batteries, or DC laboratory supply

Along with them NI SIGNAL EXPRESS DATA ACQUISITION software is required to record the data collected through NI Model USB-6009.

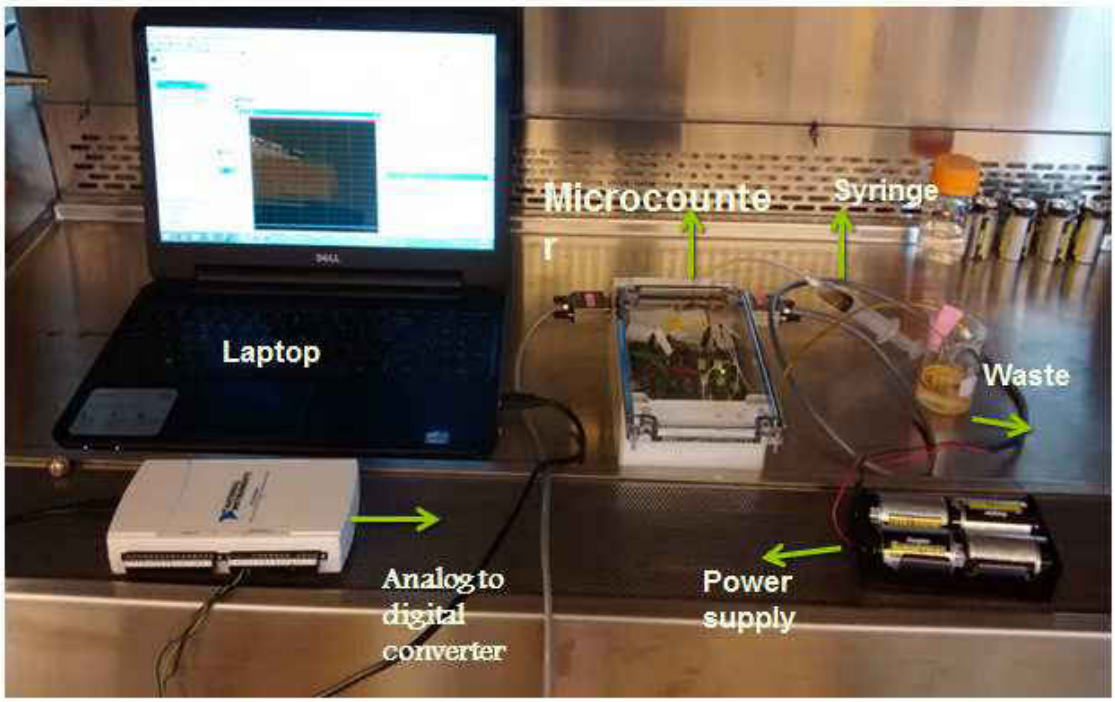

Figure 14: Experimental Setup

4.2 Ceramic beads:

Ceramic beads or Zirconium oxide beads are purchased from a local laboratory product store. For detection purpose, 0.1g of beads are weighed and mixed in 3mLs of 5W30 motor oil. While mixing it is made sure, there is no formation of air bubbles in the oil. Air bubbles create spikes if they are presented in oils. Air bubbles do block the light that is passing through the channel; it is made sure the sample is free of air bubbles.

The fluid is passed through the micro-counter manually with the help of a syringe at 3mL/min flowrate. Micro counter will start giving readings for each bead that is passed through the inbuilt light source. The signal that is received from peak detector in micro-counter is collected by SIGNALEXPRESS toolkit. It acquires, generates, analyzes, loads and store signals. The recorded data can be seen on Microsoft Excel as below.

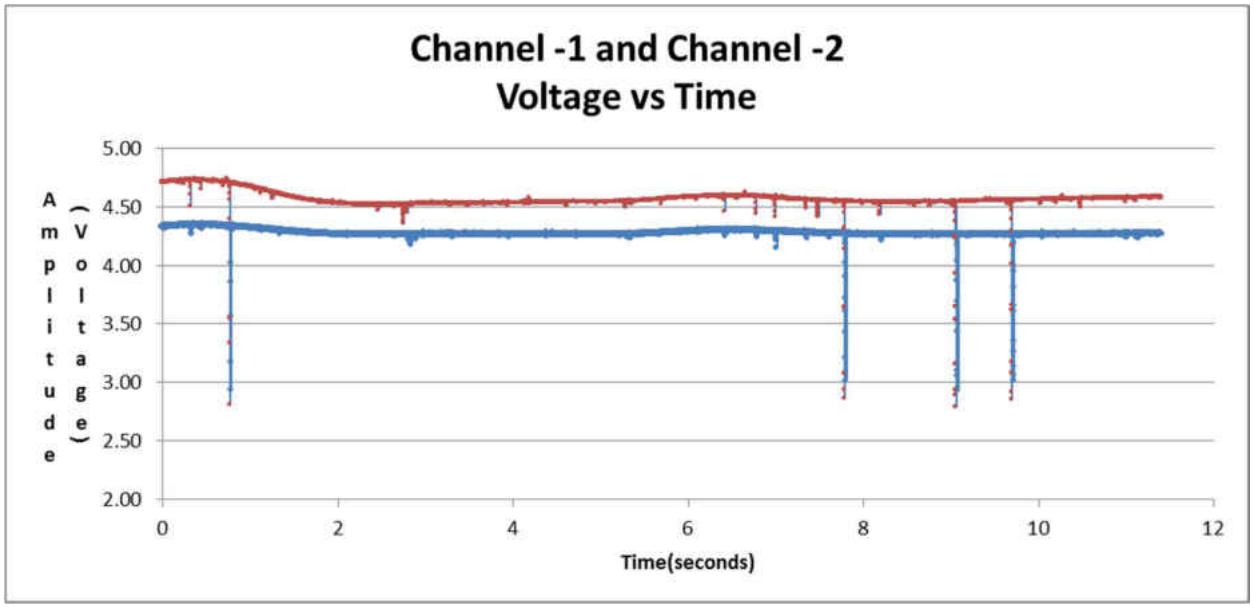

Figure 15: Ceramic beads detection (overview of the entire recorded 100µm bead data)

In the above graph, it shows channel-1 (red) and channel-2(blue) showing the beads detection in motor oil. There is spike formation for possible detection. If the, 100µm bead passes through the center of the channel, the spike would be significantly large and visible in both channels. However, if, it is moving on one side of the channel, then spike will be small on one channel and larger on the other channel.

To know the precise value of voltage difference before detection and after detection, one need to expand the data to see the values as shown in the below graph:

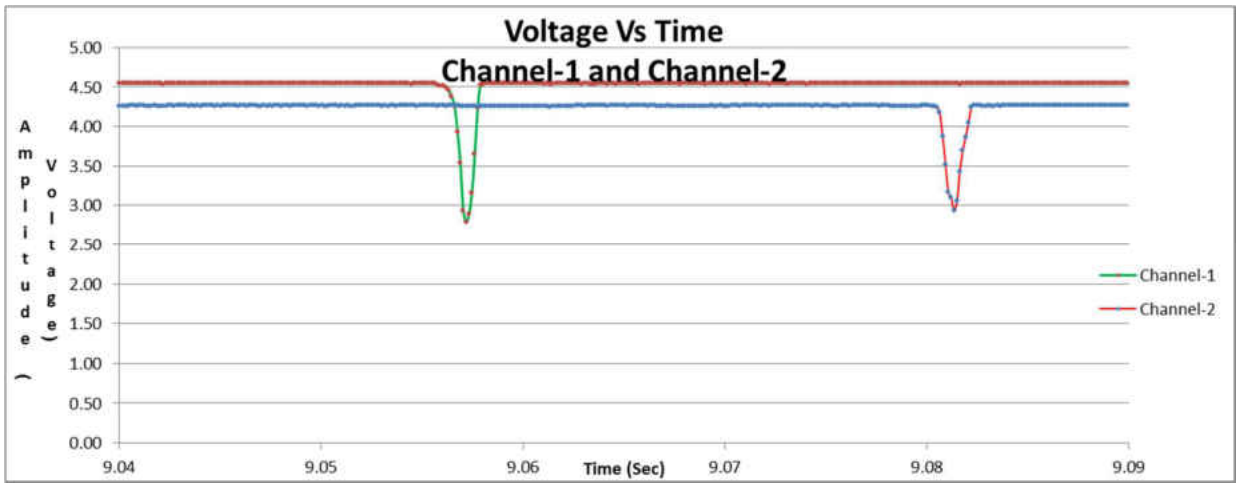

Figure 16: Close view and lapping two channels from figure 14.

In channel -1 the voltage dropped from 4.55V to 2.79V with a voltage difference of ~1.76V and in the Channel-2 the voltage dropped from 4.26V to 2.93V with a voltage difference of ~1.33V. The particle travel time from channel-1 to channel-2 took ~0.02 seconds. The noise is less in this test and data is clean with detection. This has a sampling rate of 1 kHz.

Some of the previous tests performed on micro-counter using different sizes of ceramic beads and air bubbles (diameter of approximately the tubing diameter (1/16”) or slightly less) and bacteria show significant variation in detection. Below figures represent the variation.

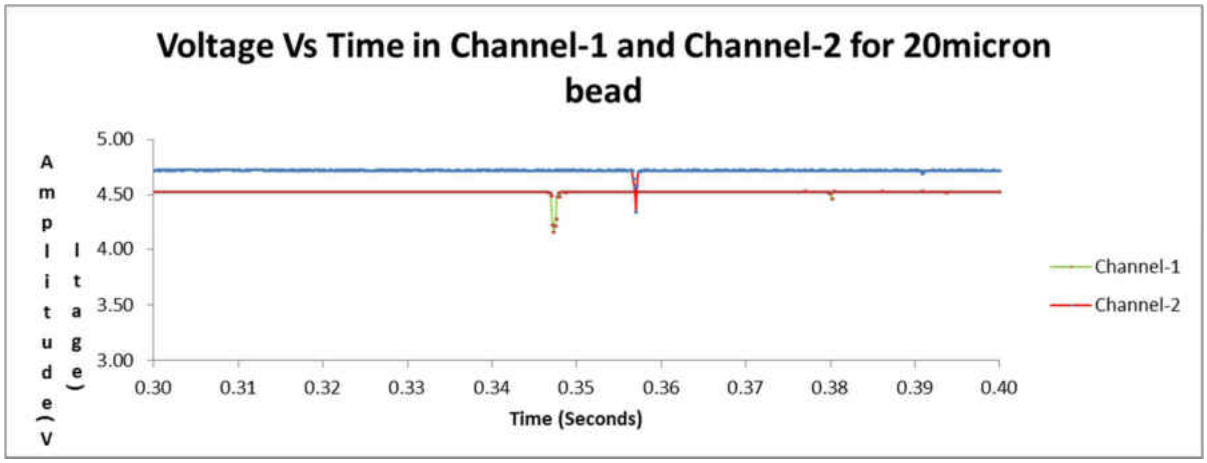

Figure 17: The voltage drop for 20 micron beads in channel-1 and channel-2 was~0.35V

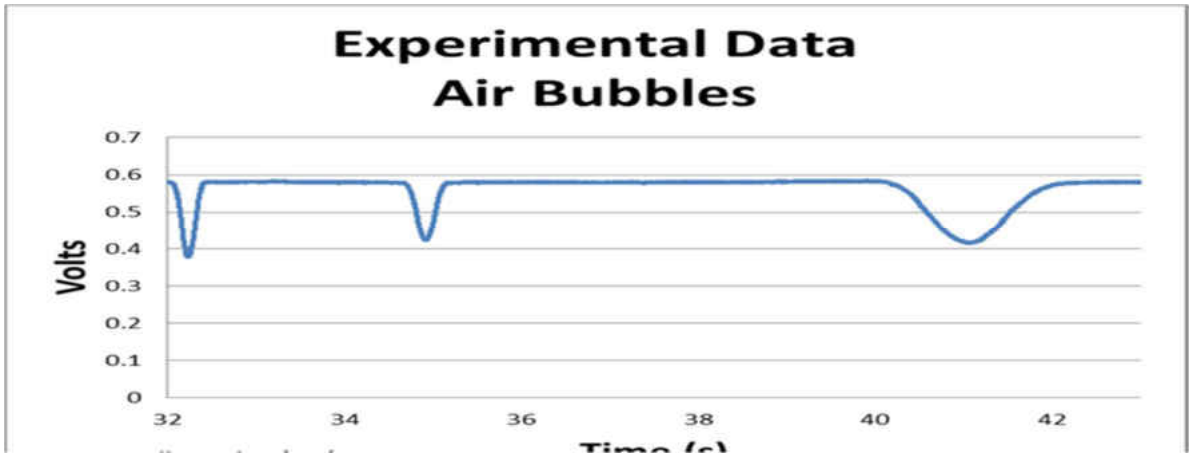

Figure 18: The voltage drop for a water bubble in channel-1 was~0.2V

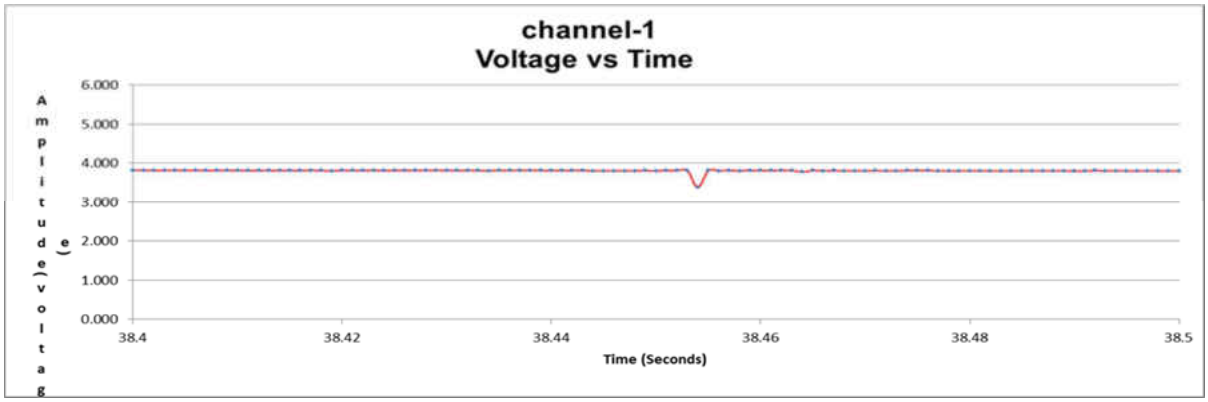

Figure 19: The voltage drop for Pseudomonas aeruginosa in channel -1 was ~ 0.022V

4.3 Pseudomonas aeruginosa

A frozen stock of Pseudomonas aeruginosa bacteria was streaked out onto a sterile tryptic soy agar plate and incubated in a 37°C incubator for 24-48hours. 5mLs of sterile tryptic soy broth was inoculated with a single Pseudomonas aeruginosa colony from the agar plate and incubated overnight in a 37°C incubator with aeration. Confirm that the OD600 is > than 1.0 and used them in the following experiment.

The 5mLs of broth was centrifuged at 3000rpm for 5mins and the supernatant was discarded, to collect the pellet of bacteria. The pellet was dried overnight to avoid water in oils. For detection purpose, the dried bacteria pellet from 5mLs broth was mixed in 3mLs of 5W30 motor oil. While mixing care was taken to avoid formation of air bubbles in oil. Air bubbles create spikes if are presented in oils.

The fluid is passed through the micro-counter manually with the help of syringe 3L/min fluid is passed through the micro counter. Micro counter will start giving readings for each bacterium that is passed through the inbuilt light source. The recorded data can be seen on Figures 15 and 16 below

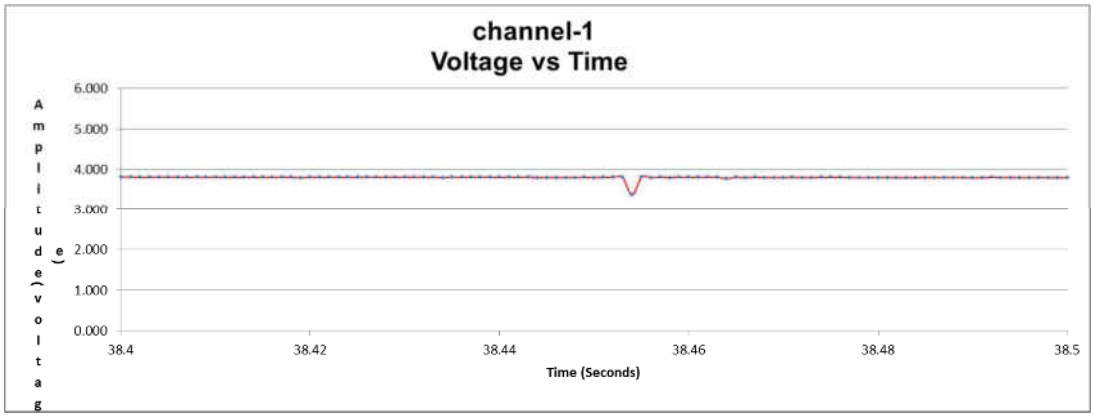

Figure 20: Closer look of Channel 1 from 38.4 seconds to 38.5 seconds with bacteria detection

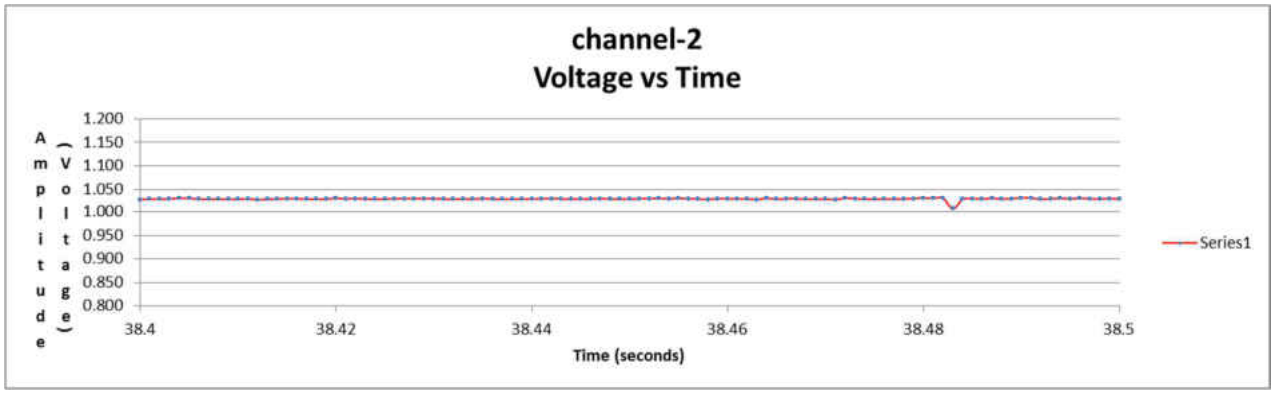

Figure 21: Closer look of Channel 2 from 38.4 seconds to 38.5 seconds with bacteria detection

In channel-1 the Voltage was dropped from 3.819V to 3.788V with a voltage difference of ~0.022V and in the Channel-2 the spike was dropped from 1.029V to 1.007V with a voltage difference of ~0.022V. The particle travel from one channel to second channel, it took ~0.02 seconds. The noise is low in this test, and data is clean with detection. As the detection is small, both were unable to get into same graph.

4.3.1 Pseudomonas aeruginosa growth curve

Another four tests with Pseudomonas aeruginosa was performed with time intervals of T1, T3, T5, and T7. These four intervals represent the days from the point bacteria is cultured in oil. For these four tests, absorbance was one of the main criteria to check the presence and concentration of bacteria in the sample that is run through the system. The experimental setup was mentioned in Appendix-A. Absorbance was taken to find the difference in change in oil color after bacterial growth. So, it was spun to clear out the bacteria or media particles that are present during the absorbance-1. Graphical data of bacteria with noise less samples are given below. In some samples noise was higher than detection, so they were excluded.

Main problem faced during following set of experiments was noise. Noise is a random fluctuation of electrical signals that are generated from electric circuits. There are five different

noises, thermal noise, shot noise, flicker noise, popcorn noise and excess noise. Tried to find, the noise generated source from our device goes to the above category but unable to figured out [9].

Results from time point 1, 24 hours after the bacteria were suspended in oil are shown in the table and charts below.

- T1 represents the 1st day of the test at 7th of April 2015.

Time Point T1	Absorbance-1 before centrifugation	Absorbance-2 After centrifugation	Average difference in absorbance
A	0.002 A	Not enough sample to retrieve	unknown
B	0.003 A	0.000A	0.0015A
C	0.053 A (sample is mixed with media)	0.000A	0.0265A
D	0.000A	0.000A	0A

Table 2: Absorbance of T1 day of A, B, C, D samples

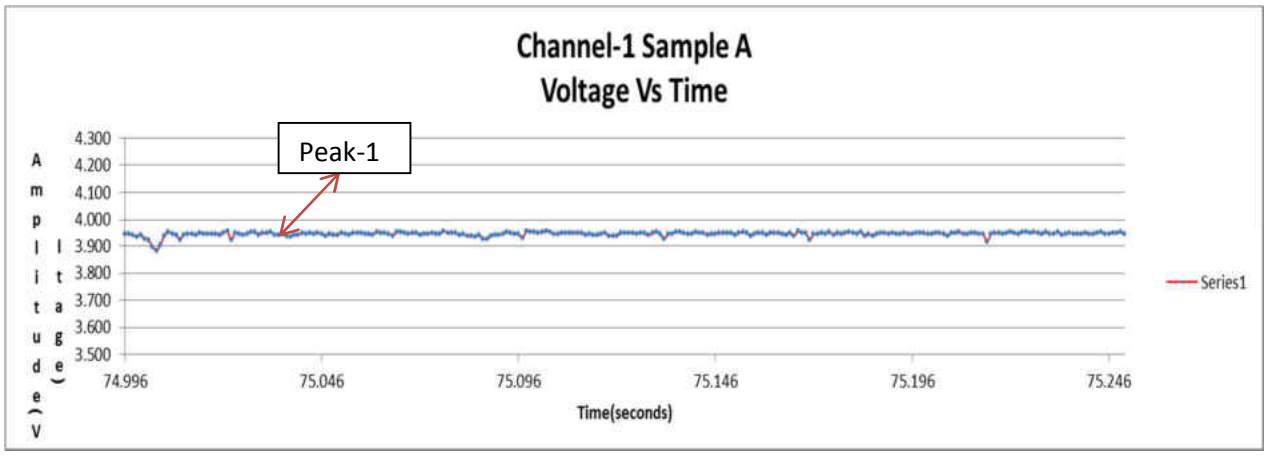

Figure 22: Closer view of Channel 1 with bacteria detection

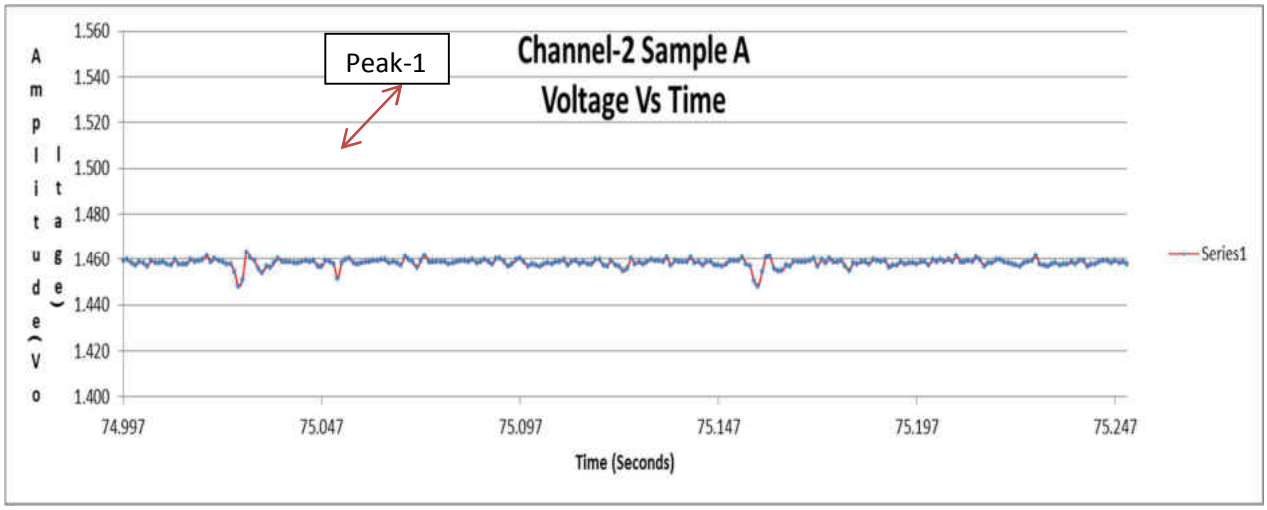

Figure 23: Closer view of Channel 2 with bacteria detection

The voltage drop of a single bacteria observed in channel-1 (peak-1) from 3.941V to 3.897V and difference of ~0.044V and for channel-2(peak-1), it is from 1.458V to 1.448V of ~0.01V. As the voltage drop for bacteria is small, when someone tries to view from entire data, they will be miss the small voltage drops. For this reason, a particular time period closer view was taken to show them in graph clearly. Unable to count the frequency of bacteria, as it was dominated by noise from the device in some time period.

- T3 represents the 2rd day of the test at 8th of April 2015 (2 days after the bacteria was suspended in oil).

Time Point T3	Absorbance-1 before centrifugation	Absorbance-2 After centrifugation	Average difference in absorbance
A	0.004 A	0.000 A	0.002 A
B	0.005 A	0.000A	0.0025 A
C	0.007A	0.007A	0.007 A

D	0.006A	0.007A	0.0065 A

Table 3: Absorbance of T3 day of A, B, C, D samples

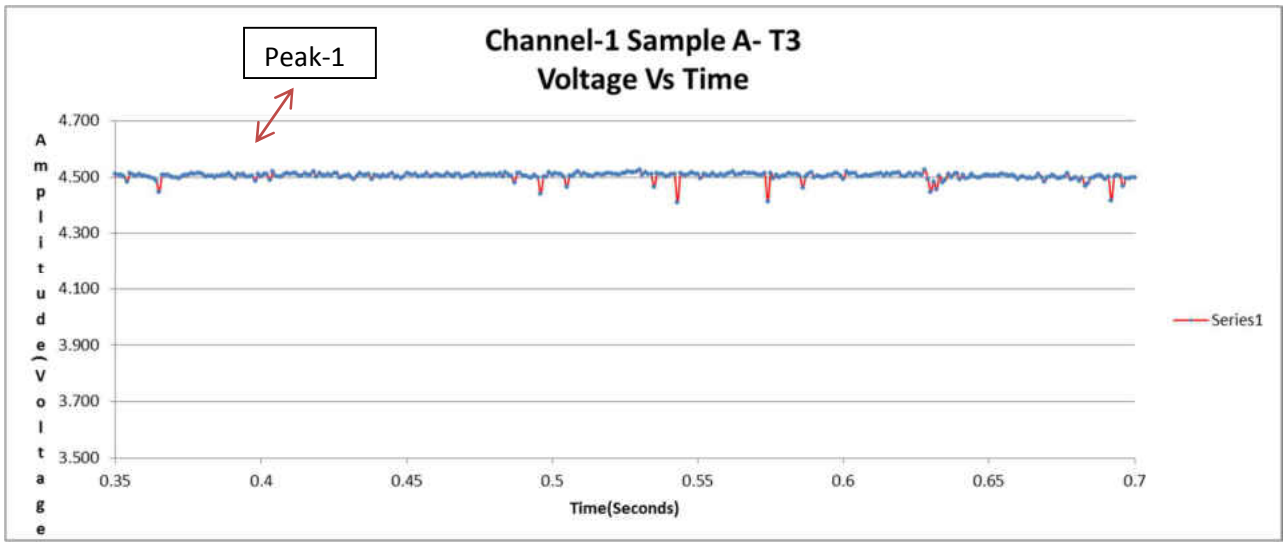

Figure 24: Closer view of Channel 1 with bacteria detection

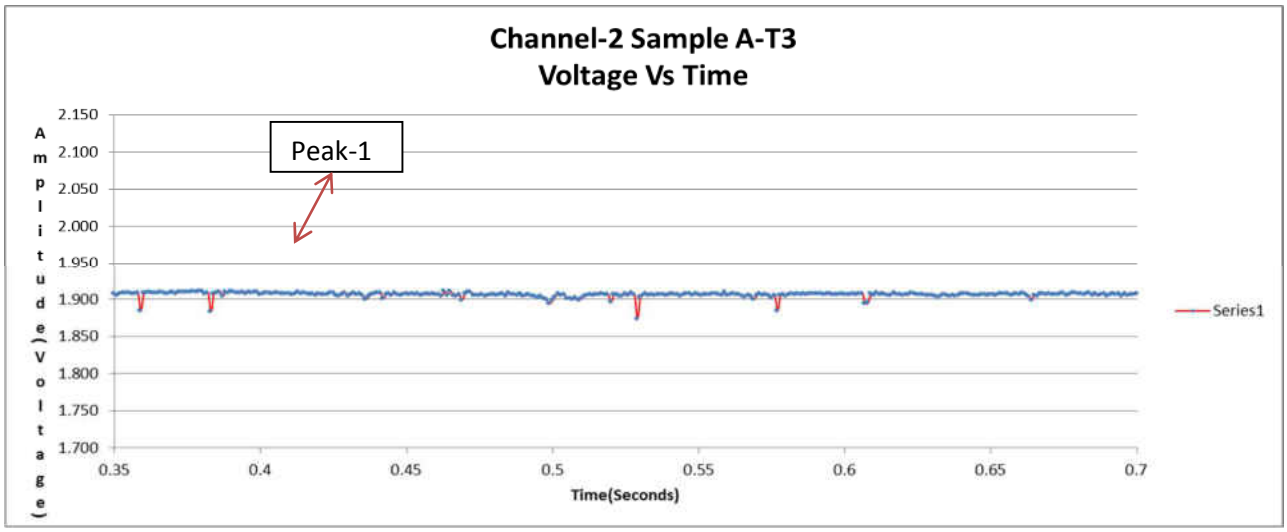

Figure 25: Closer view of Channel 2 with bacteria detection

For a single bacterium, in channel-1(peak-1) the voltage changed from 4.498V to 4.447V and a difference of ~0.051V and in Channel-2(peak-1) the Voltage was changed from 1.911V to

1.883V and with a difference of ~0.028V. The other samples have noise along with data, so they were not included here.

- T5 represents the 3rd day of the test at 9th of April 2015 (3 days after the bacteria was suspended in oil).

Time Point T5	Absorbance-1 before centrifugation	Absorbance-2 After centrifugation	Average difference in absorbance
A	0.005 A	0.001A	0.003 A
B	0.003 A	0.003A	0.003 A
C	0.038A	0.000A	0.019 A
D	0.239A	0.007A	0.123 A

Table 4: Absorbance of T5 day of A, B, C, D samples

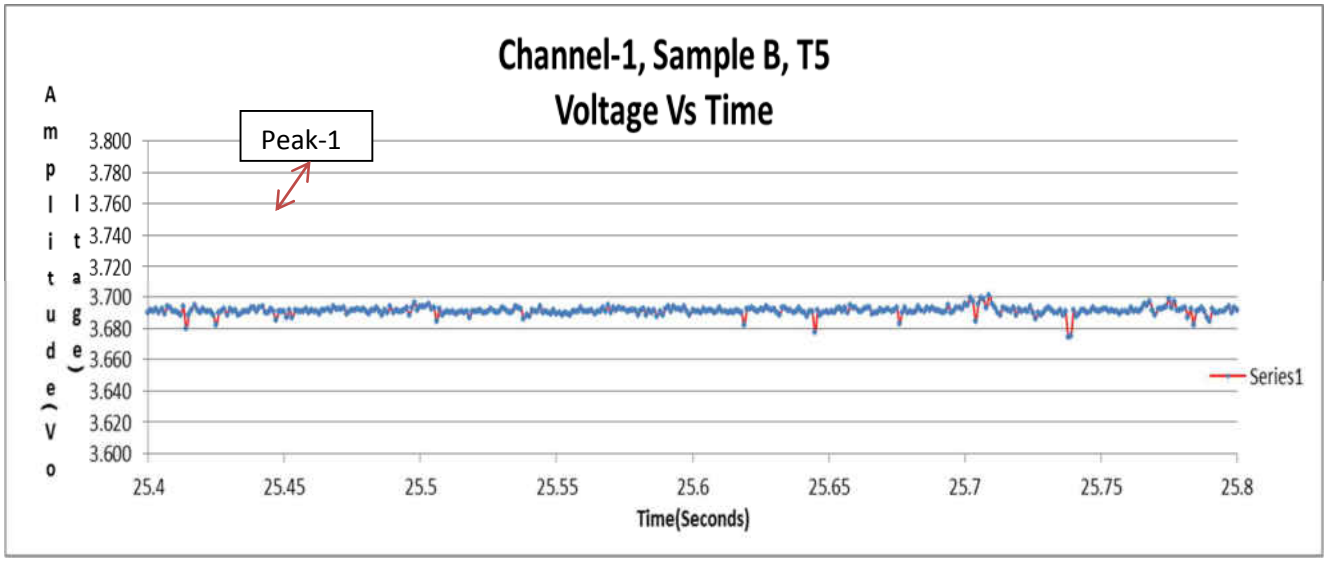

Figure 26: Closer view of Channel 1 with bacteria detection

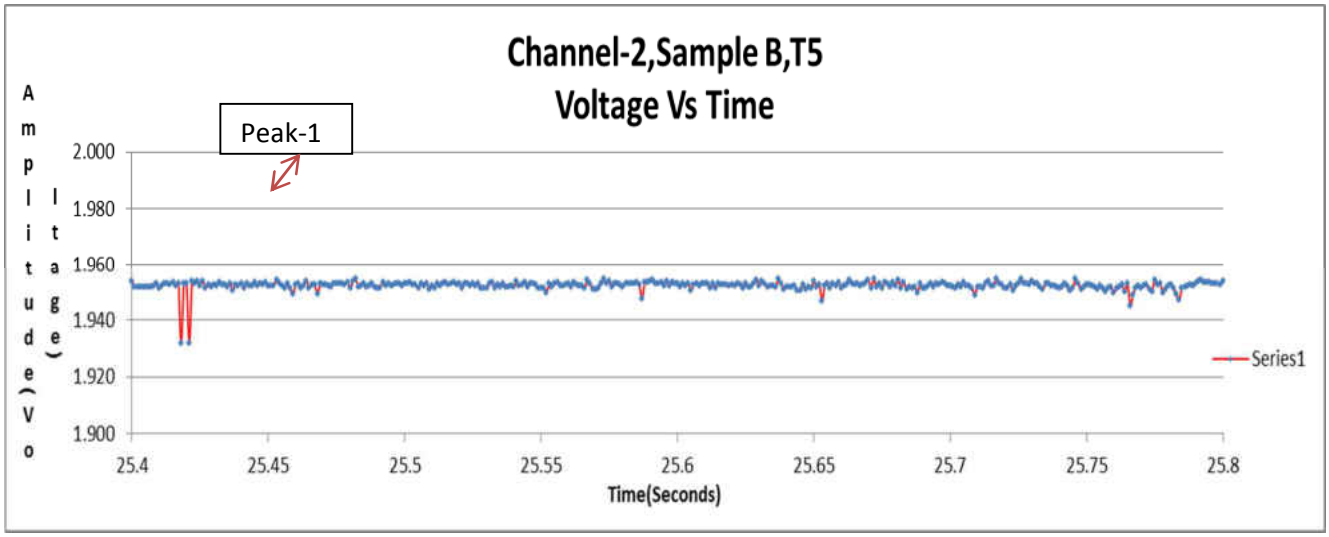

Figure 27: Closer view of Channel 2 with bacteria detection

For a single bacterium, in channel-1(peak-1), spikes are formed from 3.690V to 3.679V and voltage difference of 0.007V and in channel-2(peak-1); spikes are formed from 1.953V to 1.932V and difference of ~0.021V.

- T7 represents the 4rth day of the test at 10th of April 2015 (4 days after the bacteria was suspended in oil).

Time Point T7	Absorbance-1 before centrifugation	Absorbance-2 After centrifugation	Average difference in absorbance
A	0.008 A	0.005A	0.0065 A
B	0.018 A	0.012A	0.015 A
C	0.137A	0.084A	0.1105 A
D	0.224A	0.002A	0.113 A

Table 5: Absorbance of T7 day of A, B, C, D samples

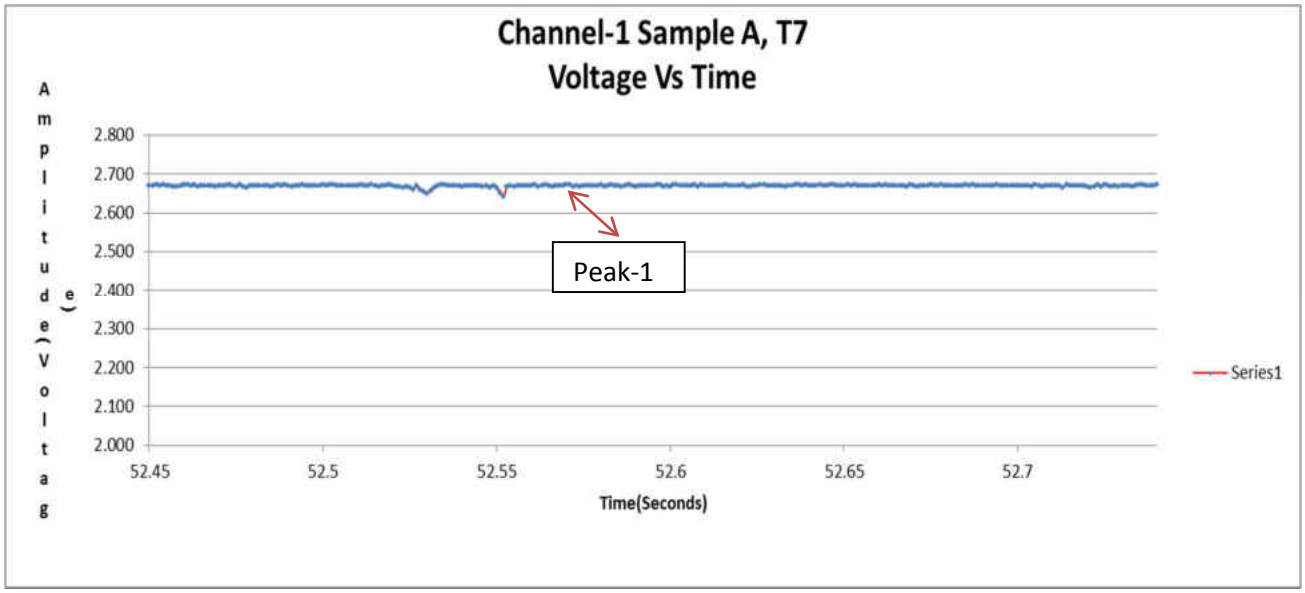

Figure 28: Closer view of Channel 1 with bacteria detection

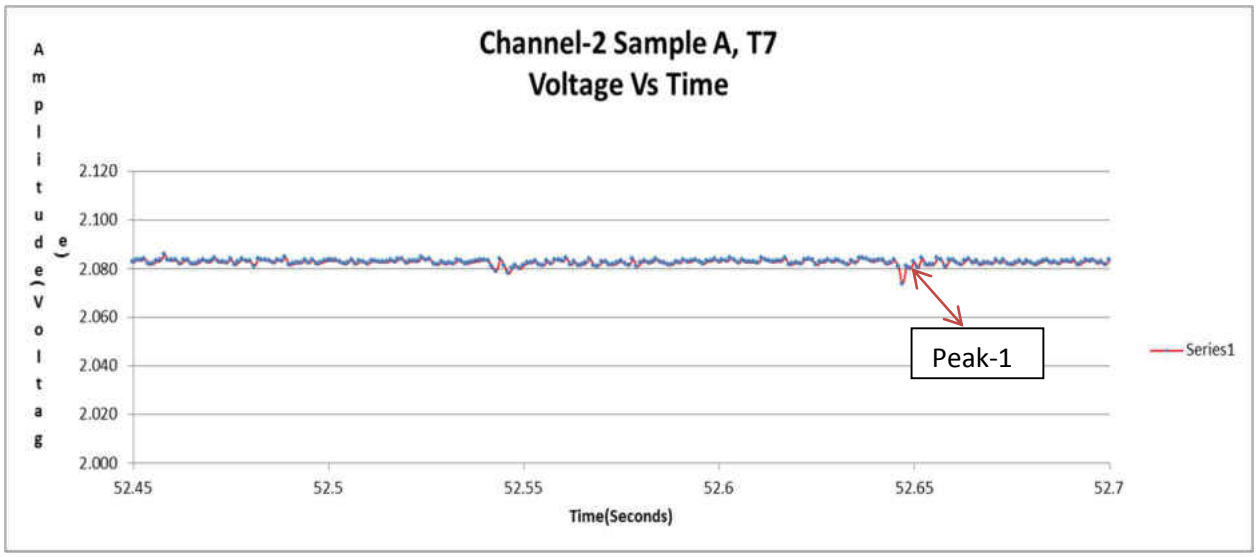

Figure 29: Closer view of Channel 2 with bacteria detection

For a single bacterium, in channel-1(peak-1), spikes are formed from 2.665V to 2.652V and voltage difference of 0.013V and in channel-2(peak-1); spikes are formed from 2.084V to 2.070V and difference of ~ 0.014V.

4.4 Discussion

The detection of bacteria is much more sensitive compared with ceramic beads. The voltage difference values are lower and require extra attention to analyze the data that is obtained. It did detect bacteria in both channels showing less voltage drop than with ceramic microbeads.

To evaluate the accuracy of the micro center, the absorbance of growth of bacteria was taken in parallel with cell detection. The challenging part was that the number of bacteria was not readily known in a given sample. However the micro-counter can count and show the bacteria in the form of spikes for a particular volume of oils that is passed through it. Controlled parameters of amount of oil, time and flow rate, while recording particles detected, have a high possibility of getting clean data. It is found that flowrate of 3mLs/min oil would give a clean data, when the flowrate was increased there was a possibility of missing biologicals from the light source as they are small by micron size.

In different time points, it is observed that turbidity in sample D at T5 and T7 prior to measurement. It is believe that pseudomonas aeruginosa is moving out of the culture media and towards the nutrients of oils, when the nutrients in media were finished. It is known that motile bacteria swim towards nutrients. The vortex shape was formed might be because of orbital shaker in which was used to aid in diffusion of air into oil for bacterial growth. On the T1 and T3 time points test tubes were less turbid and oil is clear but on T5 and T7 test tubes are turbid with dense mass of media and bacteria. Turbid oil sample was looked under microscope for bacterial growth but were unable to get a clear picture because of oil viscosity.

The spike values obtained from the micro counter can be validated be scaling down the voltage difference values of ceramic particles based on the change in size. When a spike was

scale downed by 100 times, the value that is obtained is equal to the spike value that is produced by the bacteria.

Size of particle	Voltage drop
100µm (ceramic bead)	~1.76 - ~1.33V
20µm(ceramic bead)	~0.35V
200 µm (water bubble)	~0.2V
1-2µm(bacteria)	~0.022V

Table 6: Comparison table for different particles with voltage drop.

Size of particle	No. of particles per second	Velocity of particles	Flowrate of particles per sec
100µm (ceramic bead)	~ 5 particles per second	0.15 m/s	0.0135 cm^3/sec
1-2µm(bacteria) on Day-1	~10 particles per second	0.15 m/s	0.0135 cm^3/sec
1-2µm(bacteria) on Day-2	~12 particles per second	0.15 m/s	0.0135 cm^3/sec
1-2µm(bacteria) on Day-3	~20 Particles per second	0.15 m/s	0.0135 cm^3/sec
1-2µm(bacteria) on Day-4	~25 particles per second	0.15 m/s	0.0135 cm^3/sec

Table 7: Tabular of no .of particles, velocity of particles and flowrate of particles per second

There is no sufficient data for 20µm ceramic bead and air bubbles to find the number of particles, velocity of particles and flowrate of particles.

Microcounter is cleaned with isopropanol after each test to avoid the contamination. Methanol and Ethanol can used for cleaning microcounter but less concentration of it is used. Avoiding ketones such as acetone is good for microcounter as luers can't handle ketones and they melt with immediate reaction.

Figure 30: T1 samples consist of clear oil with no turbidity.

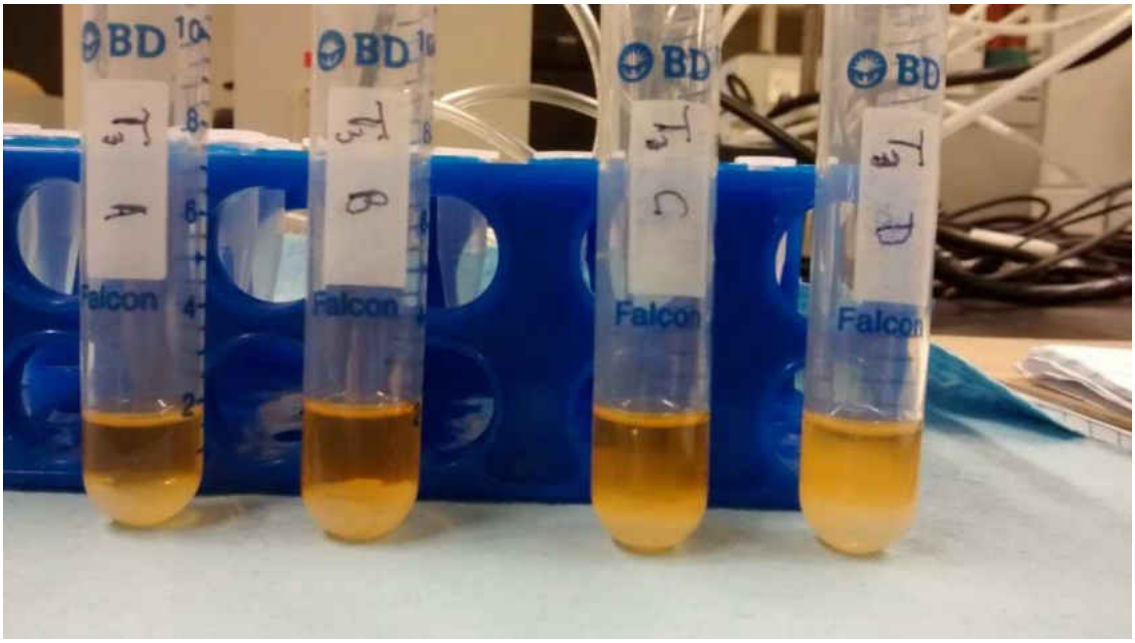

Figure 31: T3 samples; D sample is showing some change, might be bacteria growth

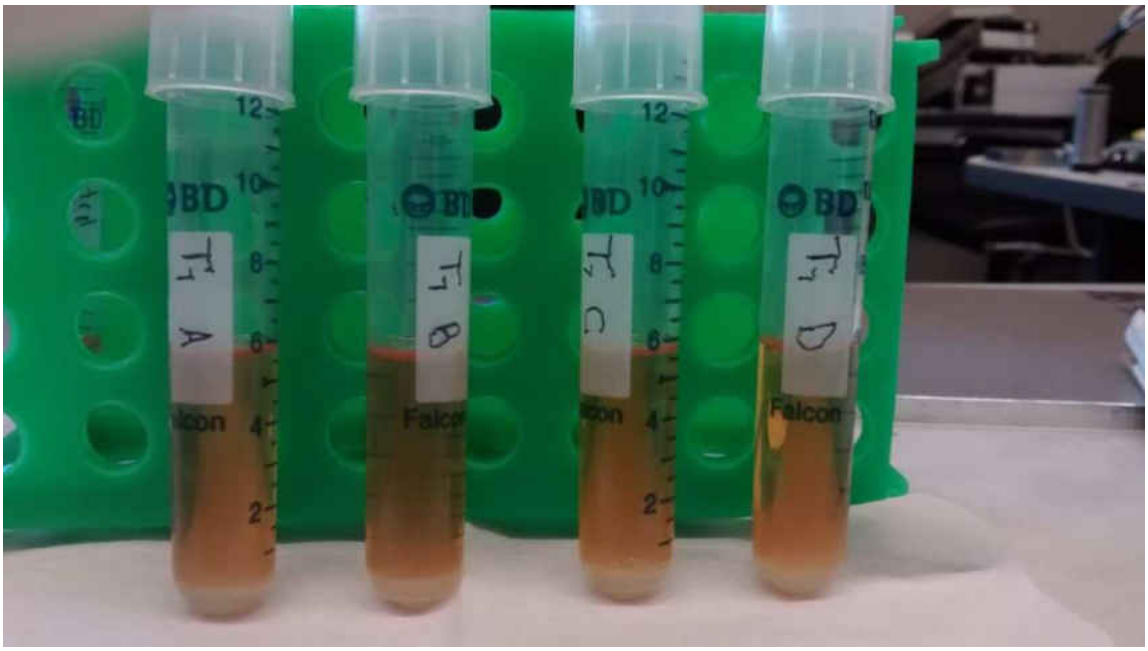

Figure 32: T7 samples, an inverted vortex shaped growth was observed on 4rth day.

There are two possibilities for it, as P.aregunosa is mobile and aerobic bacteria it might be moving upward for the air when the media is finished and that vortex shape can be because of orbital shaker.

CHAPTER 5: CONCLUSION AND FUTURE WORK

5.1 Conclusions

Detection of bacteria and ceramic beads are successfully performed using a novel micro - counter. In this study novel method was designed and developed for the detection of biologicals from the motor oils. Comparison of absorbance and detection data suggests there is growth in oil at T5 and T7 time points. In T1 and T2 time points the growth of bacteria was less; it was visible with the turbidity formation in those particular test tubes,

Some problems arose during measurement, due to because of mechanical vibrations in the biosafety hood. These mechanical vibrations affected the circuit board to produce noise along with detection data. Later one the photodiode became faulty in detecting signals from the micro counter. There was a slight problem when dust as it blocks the flow channels, caused when the lures were left open an unsanitary environment. The complete optical sensor should be covered in a box, to prevent it from environmental disturbances in future experiments.

5.2 Future work

In future work, the optical sensor sensitivity needs to be enhanced. Future, fungus need to be grown in different time points similar to bacteria and would like to test their effects on viscosity of oils and other possible biologicals that grow in oils and other fluid systems.

APPENDIX-A

Procedure for growing Pseudomonas aeruginosa and preparing samples for testing:

1. Inoculate two 5mls of sterile nutrient broth (TSB-tryptic soy broth) with a single colony from the stock bacteria streaked nutrient agar plate. Incubate overnight in a 37°C incubator with shaking (aeration).

2. Remove culture tube from incubator and take an OD600 (optical density at 600nm). Confirm that the OD600 is > than 1.0.

3. Fill 18 culture tubes with 5mls of Pennzoil SAE 5W-30.

a. Inoculate 16 tubes of oil with 500ul of bacteria in media

b. Keep two for controls

4. Place all tubes in incubator at 37°C with shaking until sample is needed for testing.

Procedure for finding absorbance:

1) Take 1ml of sample from the test tube and transfer it into a quartz cuvette.
2) Set the blank and start taking readings from the samples.
3) When absorbance values are recorded, save the sample and spin it at 3000rpm for 3 minutes.
4) Take the sample that is spun and record the absorbance values again.

APPENDIX-B

Analog circuit board design

Analog circuit board was designed by engineer Roger Alford from Translume.Inc.

1) Test Points

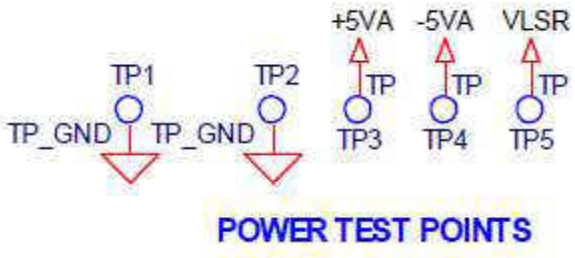

Figure I: Test points

Reference: Translume.Inc.

The PDLD Board includes five standard test points for monitoring board voltages and providing for a ground connection for probing; these are identified as TPx in the schematic and on the board. The two GND test points, TP1 and TP2, are located at remote areas of the board from each other, and can be used for oscilloscope or multimeter ground referencing; these test points are bare metal. The power test points,

TP3-TP5, are white with a metal loop and are used to monitor the on-board voltages. Here is a summary of the voltages associated with the 5 standard test points:

TP1: GND

TP2: GND

TP3: +5V

TP4: -5V

TP5: VLSR

Throughout the board there are other types of test points, referred to as test point pads (TP_PADx) on the schematic, and as TPDx on the board itself. These are plated-through holes in the board that provide useful reference locations for monitoring or otherwise accessing key signals; the holes are sized to accommodate a standard 0.025 in. square post, although this is not normally stuffed.

2) Power:

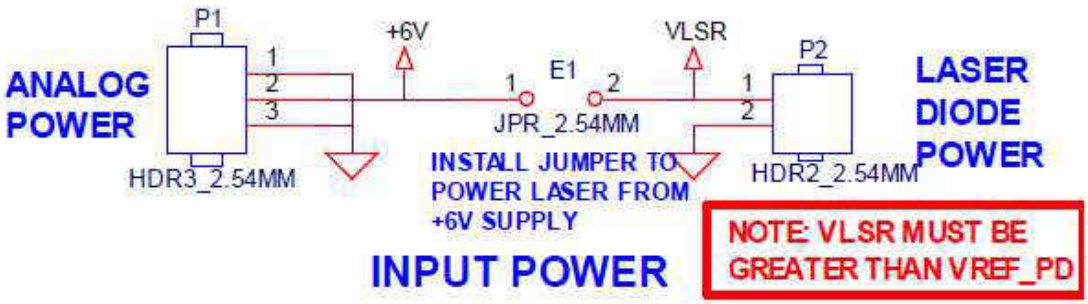

Figure II: power

Reference: Translume.Inc.

The input power to the board is intended to be nominally 6V, and is supplied to the board at connector P1; pins 1 and 3 (the outer pins) connect to ground (it is okay to connect only one ground), and the center pin (pin 2) connects to the input supply voltage. The minimum input voltage is 5.4V and the maximum is 12V, although it is recommended that the voltage not exceed 9V to minimize power dissipation in the LT1121-5 voltage regulator (U2), which generates +5V ±3% power for the board's circuits from the input power. The green LED, LED1, will light when +5V power is present. The board will normally consume less than 100mA from the +5V supply; the LT1121-5 regulator is capable of outputting up to 150mA. The power dissipated in the regulator is the difference between the input voltage and +5V, multiplied by the

current being drawn from the regulator. With 6V in and 100mA being drawn, the dissipated power is (6-5)*0.1 = 100mW. With 12V in and 100mA being drawn, the dissipated power jumps to (12-5)*0.1 = 700mW, making the regulator quite warm or hot to the touch.

The PDLD Board includes a circuit based on an LTC1261L chip that generates -5V (actually about -4.5V) from the +5V supply. The LTC1261L chip has a REG output accessible at TPD1; this signal is pulled up to +5V with a resistor and is pulled down by the chip when the chip achieves output regulation within 5% of its (-4.5V) target. The chip is normally expected to operate within regulation, so this signal should normally be low. The LTC1261L is capable of supplying a maximum of 20mA. Except for the laser diodes, all of the board's circuits are powered from the +5V and -5V supplies. The laser diodes are sourced by a separate power supply, VLSR that is normally supplied to the board at connector P2; pin 2 of this connector connects to ground and pin 1 connects to the VLSR supply voltage.

Optionally, instead of supplying a separate voltage for the laser via P2, a 0.1" jumper (shunt) can be installed at E1; this routes the (nominal 6V) board input supply voltage to the VLSR trace on the board, allowing this supply to also power the lasers. Note that only the input power supply may be routed to VLSR; the on-board regulated +5V supply may not be used to power the lasers.

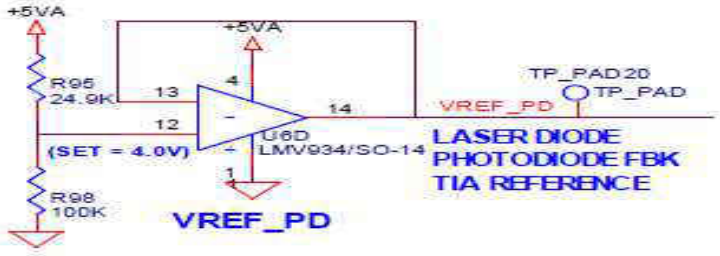

Figure III: VLSR

Reference: Translume.Inc.

There is a circuit that sets the VREF_PD voltage, which is the reference voltage for the photodiode feedback from the laser diode to allow for constant power mode operation. The VREF_PD is derived from the +5V supply via a voltage divider and is set to 4.0V by default, but can be changed by altering the voltage divider. If the photodiode feedback from the laser diode is used, it is necessary that VLSR be greater than VREF_PD by at least 0.25V.

Photodiode Circuits:

The four photodiode input circuits are nearly identical. The primary difference is that PD #3 and PD #4 include an optional pot in the feedback path of the trans impedance amp, and the amplifier output can be used to control the optical power of laser diodes LD #1 and LD #2, respectively; the pot is not included with PD #1 and PD #2. PD #1 provides the trigger signal for the integrator and peak detector circuits for all four photodiode circuits.

Photodiode Connectors

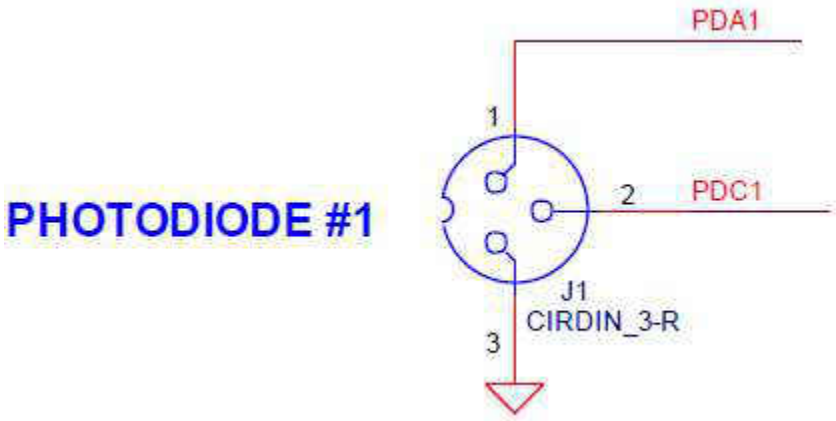

Figure IV: Photodiode

Reference: Translume.Inc.

Pin 1: ANODE (connects to -5VA)

Pin 2: CATHODE

Pin 3: CASE (ground)

Twenty-six pin header connector P4 also includes connections for all four photodiodes (and both laser diodes), allowing for photodiodes to be placed on a remote board that is then cabled or directly attached to the PDLD Board. The P4 photodiode connections are as follows:

Pin 1: Ground Pin 2: Ground

Pin 3: PD #1 CATHODE Pin 4: PD #1 ANODE

Pin 5: Ground Pin 6: Ground

Pin 7: PD #2 CATHODE Pin 8: PD #2 ANODE

Pin 9: Ground Pin 10: Ground

Pin 11: PD #3 CATHODE Pin 12: PD #3 ANODE

Pin 13: Ground Pin 14: Ground

Pin 15: PD #4 CATHODE Pin 16: PD #4 ANODE

Theory of Operation

Since all of the photodiode circuits are virtually identical, we will describe the operation of the PD #1 circuit here – including specific component reference designators – and the description will apply correspondingly to the other photodiode circuits, except as noted.

Transimpedance Amplifier (TIA):

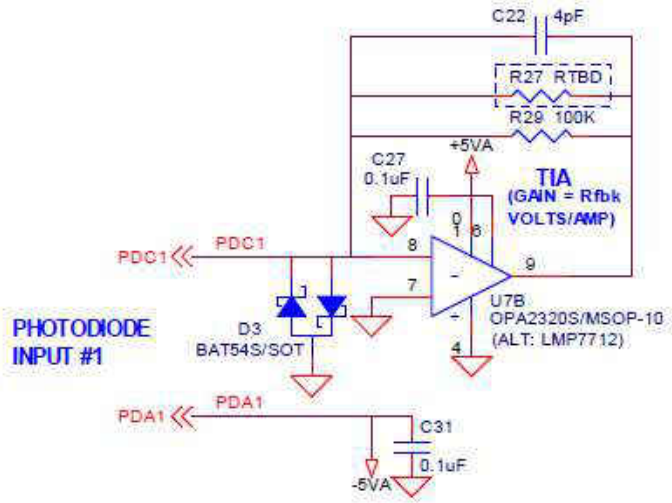

Figure V: TIA

Reference: Translume.Inc.

The photodiode connects directly to the transimpedance amplifier (TIA) to convert the photodiode current to a voltage usable by the remaining photodiode circuits. The TIA (one of the two U7 amps) is a 10-pin National LMP7712. The photodiode cathode connects to the inverting input of the amp and is held a virtual ground. The photodiode anode is connected to -5V to provide a reverse bias to the photodiode, for lower noise and faster response. The TIA feedback resistor (R29) determines the gain of the circuit in Volts/Amp; a value should be chosen based on the characteristics of the photodiode being used, such that the amplifier output goes to approximately 4.0V-4.5V when the photodiode is receiving the maximum expected light. For example, if the photodiode outputs nominally 5mA at the maximum expected light level, a resistor value of 4.25/0.005 = 850Ω provides a nominal 4.25V at the output of the TIA at this light level. Note that R29 is shown as 100kΩ on the schematic, but this is just a placeholder for a value to be determined based on the specific photodiode and expected light intensity. The Rev. A board TIA includes provision for a second, parallel feedback resistor (R27) in case this may be

helpful in adjusting the TIA gain (lower) by adding a resistor in parallel with the primary gain resistor; this provision is removed on the Rev. B board.

In the PD #3 and PD #4 TIA circuits, there is a resistor in series with a pot together in parallel with the primary feedback (gain) resistor. If the PD circuit is to be used to control the optical power of the corresponding laser diode, the primary feedback resistor should be unpopulated, and only the pot and its series resistor should be populated. The series resistor establishes a minimum TIA gain value, and the pot value added to the series resistor value establishes the maximum TIA gain. The pot, then, can be used to adjust the desired laser diode optical power level. This will be described more in the laser diode driver section.

Baseline Restore:

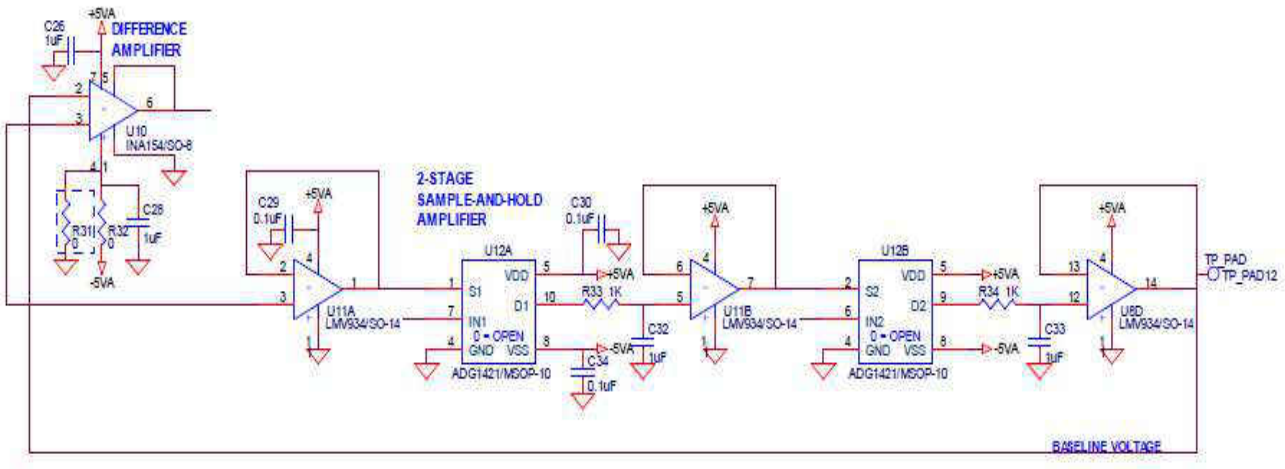

FigureVI: Baseline restore

Reference: Translume.Inc.

The output of the TIA is input to the positive terminal of an INA154 difference amplifier (U10), which is one element of the baseline restore circuit. The negative terminal of the difference amp comes from the output of a two-stage sample-and-hold amplifier (a “bucket brigade”), which establishes the baseline output of the TIA. When a trigger event occurs, the

output of the two-stage sample-and-hold amp is held at its most recent value, to maintain the baseline reference voltage throughout the integration period. After the end of the integration period, the sample-and-hold circuit updates normally. By using two stages, there is no risk of the baseline changing as the TIA output changes just prior to, or as part of, the trigger event. The Rev. A boards use 1µF hold capacitors by default, whereas the Rev. B boards use 10µF hold capacitors by default; these capacitor values can be easily changed on either revision of the board 2Hz rate.

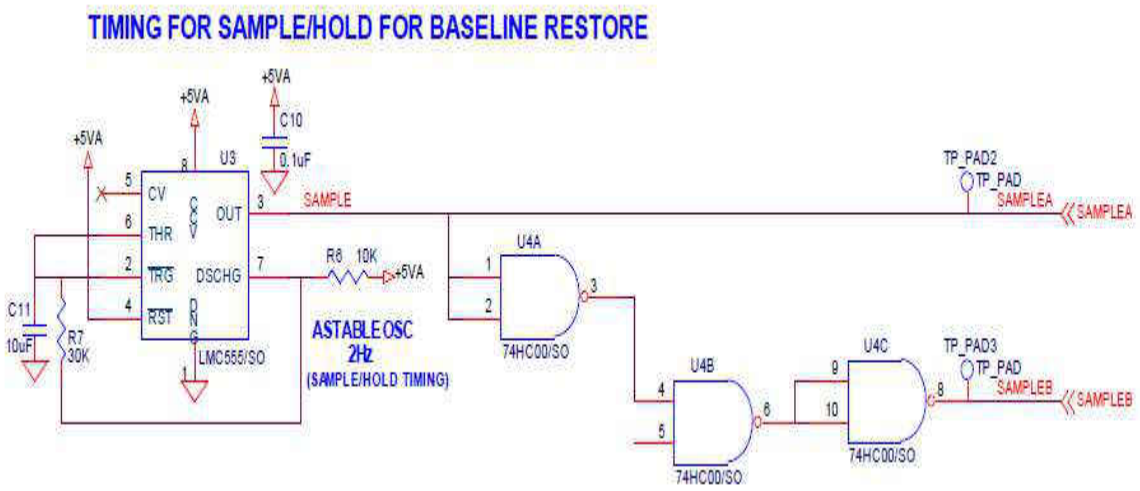

Figure VII: Timing for sample/hold for baseline restore

Reference: Translume.Inc.

Another signal, SAMPLEB, is the inversion of SAMPLEA gated with the INTEGRATE# signal. During the non-integration period, SAMPLEB is simply the inversion of SAMPLEA. When SAMPLEA is high, switch U12A is closed (Stage 1 in Sample Mode), causing cap C32 to charge to the output voltage of the TIA. During this time SAMPLEB is low and switch U12B is open (Stage 2 in Hold Mode), causing cap C33 to hold its last charge value. The voltage on C33 is buffered and input to the inverting terminal of the difference amp as the baseline reference

voltage. Since the voltage on C33 should be the same as the output voltage of the TIA, the output of the difference amp should be 0V at this time.

When SAMPLEA is low (Stage 1 in Hold Mode), cap C32 holds its last charge value, which is buffered and provided as an input to Stage 2. During this time SAMPLEB is high (Stage 2 in Sample Mode), causing cap C33 to charge to the voltage on C32. This two-stage sampling/holding occurs continuously during the non-integration time. When a trigger event occurs initiating the integration time, the INTEGRATE# signal goes low forcing SAMPLEB to go low (or stay low), allowing C33 to maintain the baseline reference voltage for the duration of the integration period. At the completion of the integration period, INTEGRATE# returns high and the normal two-stage sample-and-hold baseline operation resumes. During the integration period, then, the difference amp outputs the difference between the baseline voltage and the TIA output voltage, providing only the voltage that is greater than the baseline voltage. The output of the difference amp connects to the Analog Outputs connector (P3) as the TIA_BASELINEDx signal, and is also the input signal to the integrator and the peak detector circuit. The buffered output of sample-and-hold Stage 2 is accessible at test point pad TPD12; signal SAMPLEA is accessible at TPD2; signal SAMPLEB is accessible at TPD3; and signal INTEGRATE# is accessible atTPD4.

NOTE: Stage 1 (only) of the two-stage sample-and-hold amplifier continues to sample and/or hold just before and during the integration period. It is therefore possible that an incorrect baseline voltage is stored in the Stage 1 cap at the end of the integration period, which then gets propagated to the Stage 2 cap, temporarily establishing an incorrect baseline voltage. Assuming the TIA has returned to the proper baseline level, the baseline restore circuit will self-correct for this within 600ms after the end of the integration period; however, a new trigger event may occur

before the baseline voltage is corrected, resulting in incorrect output signal levels. As described in the section Revision A to Revision B Changes, the Rev. B design defaults to a 20 Hzoscillator frequency, compared to the 2 Hz default on the Rev. A boards. This frequency can be easily changed on either of the boards. The Rev. B board design also qualifies the signal SAMPLEA with the INTEGRATE# signal to keep the first stage of the sample-and-hold amplifiers in sample mode during the periods when INTEGRATE# is asserted; the Rev. A board assemblies incorporated this change via manual rework.

Integrator:

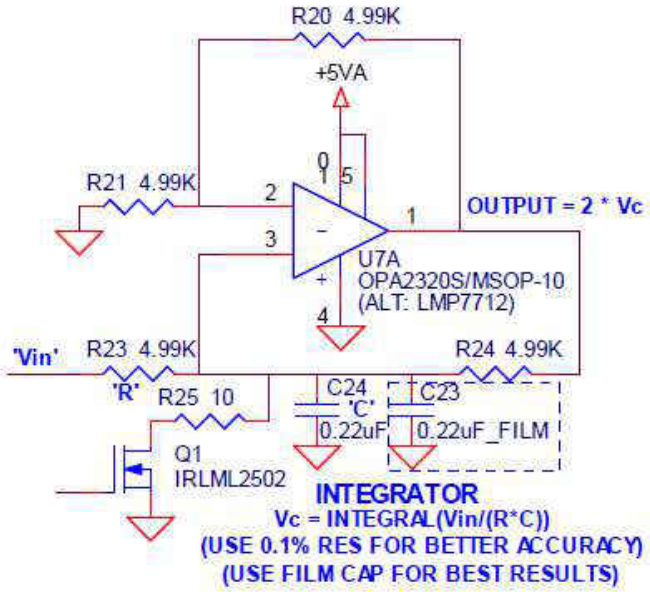

Figure VIII: Integrator

Reference: Translume.Inc.

The Deboo integrator circuit operates on a single power supply (+5V) and easily allows the integration cap to be discharged ("reset"). The integrator uses the second LMP7712 (U7) amplifier (the first is used by the TIA circuit).

The integrator circuit includes two integration capacitor footprints, one for a small 0603 surface mount ceramic cap (C24) and one for a through-hole film type cap (C23). The film cap

has lower leakage and therefore results in a more accurate integration. The ceramic cap is smaller, cheaper, and easier to work with to experiment with different values. Only one cap or the other should be installed at any given time, not both. The cap value (C) determines the how rapidly the voltage increases at the determined charge rate.

Four equal-value (R) resistors (R20, R21, R23 and R24) set the integrator charge rate as function of the input voltage from the difference amp (Vin). The voltage on the integration cap, Vc, as a function of time is:

$Vc(t) = 1/(R*C) * \int Vin(t)\, dt$

The output of the integrator is 2 * Vc(t).

The standard value for R, as shown in the schematic, is 4.99kΩ. With the default 0.22uF cap value, 1/(R*C) = 911. With these R/C values, a constant input voltage Vin of 1V will integrate to Vc = 2.5V (integrator saturation) in about 2.7ms. A larger cap value will result in slower (longer) integration, whereas a smaller cap value will result in faster integration. The cap value should be selected based on the expected input voltage and the desired integration time. If necessary the four integrator resistors can be changed, but they should all be kept at the same value. These resistors can be 1% tolerance if integrator accuracy is not especially important, but 0.1% tolerance resistors are recommended for more accurate integration. During the non-integration period (INTEGRATE# signal is high), FET Q1 is switched on, discharging the integration cap through R25. After a trigger event and the activation of the integration period (INTEGRATE# signal low), FET Q1 is switched off, allowing the integration cap to charge as described above.

The Rev. A board design defaults to 4.99KΩ, 0.1% resistors for the integrator gain, whereas the Rev. B board design defaults to 10kΩ, 0.1% resistors. The Rev. A and Rev. B board

assemblies both default to using a 1.0µF FILM integration capacitor. So the default 1/(R*C) value for the Rev. A boards is 200, and 100 for the Rev. B boards; thus, the integrator output of the Rev. A boards will ramp up twice as fast as those on the Rev. B boards. The integration values on either board can be easily changed by changing the integration resistor and capacitor values. The output of the integrator is buffered and output to the Analog Outputs connector (P3) as the INTEGx signal.

Peak Detector:

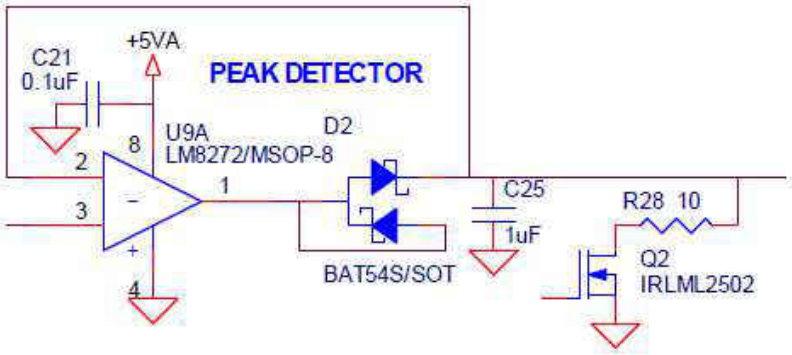

Figure IX: Peak Detector
Reference: Translume.Inc.

The peak detector circuit uses an LM8272 op amp because of its high current output capability and suitability for directly driving highly capacitive loads. The output of the difference amp provides the input to the peak detector. During the integration period, capacitor C25 is charged to the peak voltage from the difference amp, holding this voltage for the remaining duration of the integration period. During the non-integration period (INTEGRATE# signal is high), FET Q2 is switched on, discharging the peak detector cap through resistor R28. The output of the peak detector is buffered and output to the Analog Outputs connector (P3) as the PEAKx signal.

The peak detector cap, C25, is normally 1uF, which is expected to be a good value for this system based on the anticipated signal levels and timing. For faster circuits, a smaller cap

value can be used to allow for faster charging, although this will result is faster droop (the inability to hold the charge for a long period of time due to leakage currents). For slower circuits, a larger cap value can be used, resulting in a longer charge hold-up time (less effect from leakage currents).

Trigger:

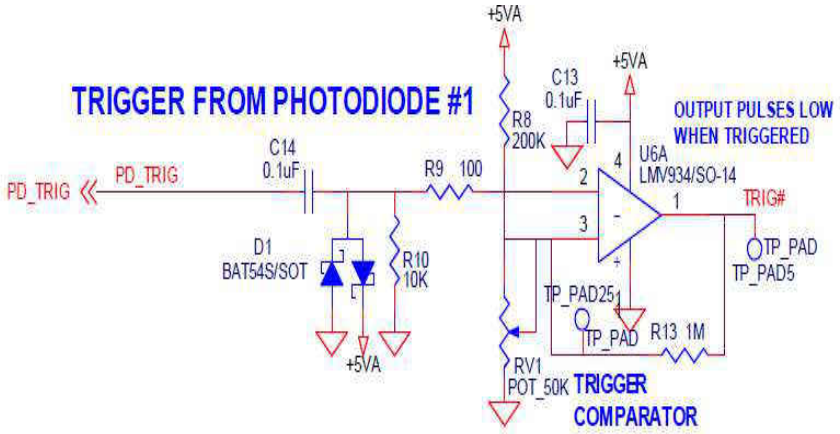

Figure X: Trigger

Reference: Translume.Inc.

The PD #1 TIA is the source of the trigger for initiating the integration and peak detection for all four photodiode channels. The non-baselined TIA output from PD #1 is provided to the trigger circuit on schematic Sheet 1. The signal is AC coupled via capacitor C14; R10 keeps the signal downstream of the cap ground referenced during the non-trigger periods, and diode D1 acts as a clamp to keep the downstream signal from going below ground by more than a diode drop when the trigger signal from the TIA falls.

The AC-coupled trigger signal is input to the inverting input of an LMV934 type op amp (U6A) configured as a comparator. The non-inverting input of the comparator connects to a voltage divider, with pot RV1 used to adjust the trigger threshold; with a 50kΩ pot and a 200kΩ pull-up resistor, the trip threshold voltage ranges from 0V to about 1.1V. By default the threshold

should be adjusted to about 0.2V, but a more optimal value may be determined empirically. TPD25 provides access to the trip voltage while adjusting the pot.

The output of the comparator is normally high, but goes low briefly when a trigger signal is received. The low pulse from the comparator is input to an LMC555 timer chip configured as a one-shot for timing the integration period. The LMC555 requires a minimum low trigger pulse time of 20ns. The comparator circuit provides nominally 100mV of hysteresis via the 1MΩ positive-feedback resistor, which helps lengthen the output pulse width by adjusting the input trip threshold lower after the output transitions from high to low. The output of the trigger comparator is accessible at TPD5. As described in the section Revision A to Revision B Changes, the Rev. B design enhances the trigger circuit design compared to Rev. A, particular to add support for negative-pulse triggering.

Integration Period Timing:

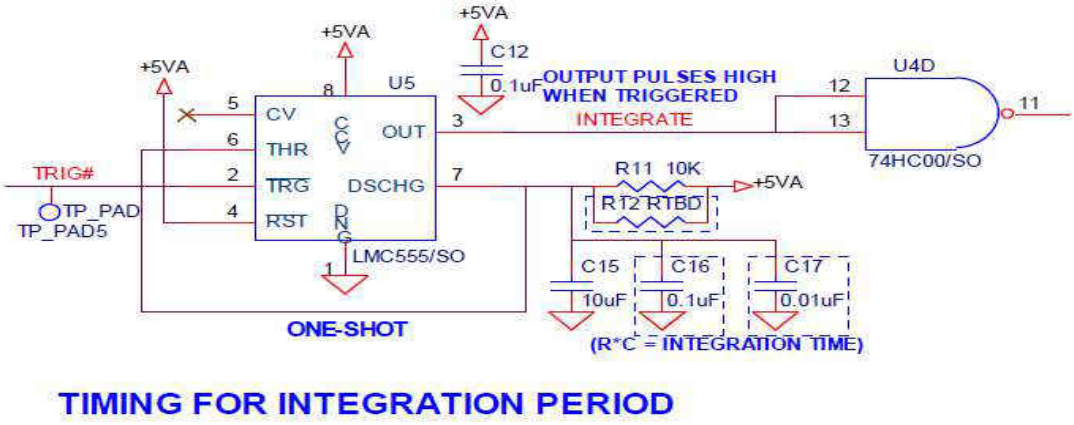

Figure XI: Timing for Integration Period

Reference: Translume.Inc.

The output of the trigger comparator triggers the LMC555 configured as a one-shot, the output of which is the INTEGRATE# signal that determines the length of the integration period. INTEGRATE# is normally high before a trigger event occurs. When a trigger pulse is received,

INTEGRATE# goes low for the period of time determined by the values of the timing resistor(s) and capacitor(s). INTEGRATE# is accessible at TPD4.

Resistor R11 is the standard timing resistor. Optionally a second resistor, R12, may be installed, in which case the effective timing resistance is the parallel resistance of the two resistors. Capacitor C15 is the standard timing capacitor. Optionally cap C16 and/or cap C17 may be installed in addition to or instead of C15. If more than one cap is installed, the effective timing capacitance is the sum of the installed capacitances. The integration period is determined by the product of the effective timing resistor and the effective timing capacitor. Thus, for example, if R11 is 4.7kΩ and C15 is 10μF and these are the only installed timing elements, the integration period will be approximately 4.7E3 * 10E-6 = 47ms. The flexibility in resistor and capacitor values allows for a wide range of integration period timing, from microseconds to seconds.

Analog Outputs:

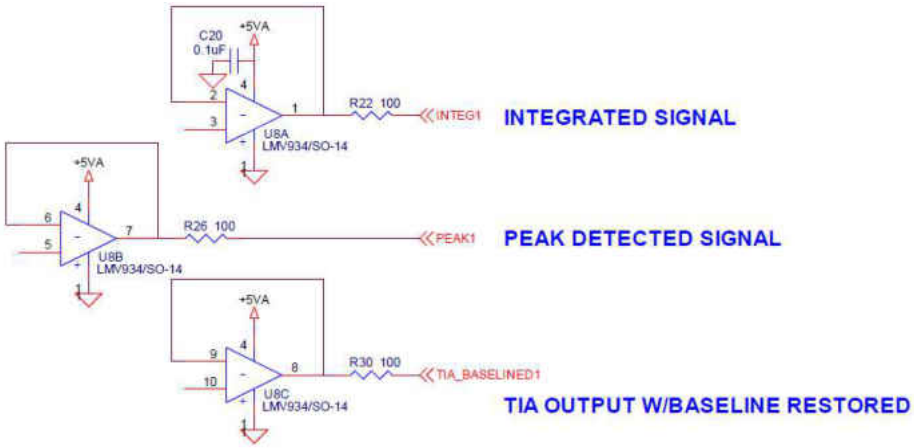

Figure XII: Analog Outputs

Reference: Translume.Inc.

The INTEGRATE# signal and the three outputs from each photodiode circuit are all routed to Analog Outputs connector P3, a 20-pin header connector; the three analog signals are all buffered with LMV934 op amps. The P3 connections are as follows:

Pin 1: Ground Pin 2: Ground

Pin 3: TIA_BASELINED1 Pin 4: TIA_BASELINED2

Pin 5: PEAK1 Pin 6: PEAK2

Pin 7: INTEG1 Pin 8: INTEG2

Pin 9: (no connect) Pin 10: INTEGRATE#

Pin 11: Ground Pin 12: Ground

Pin 13: INTEG3 Pin 14: INTEG4

Pin 15: PEAK3 Pin 16: PEAK4

Pin 17: TIA_BASELINED3 Pin 18: TIA_BASELINED4

Pin 19: Ground Pin 20: Ground

Laser Diode Driver Circuits:

The two laser diode driver circuits are identical. Each has a choice of three different control signal sources, allowing for constant-current or constant optical power drive. One control input source is from an on-board pot used to set the constant current level through the laser diode. The second control input source uses feedback from a photodiode integrated in the laser diode – in conjunction with a TIA pot – to establish a constant-power setting for the laser diode. The third control input source uses the output from the PD #3 (for LD #1) or PD #4 (for LD #2) TIA to establish a constant-power setting for the laser diode.

Laser Diode Driver Circuits:

The two laser diode driver circuits are identical. Each has a choice of three different control signal sources, allowing for constant-current or constant optical power drive. One control input source is from an on-board pot used to set the constant current level through the laser diode. The second control input source uses feedback from a photodiode integrated in the laser diode – in conjunction with a TIA pot – to establish a constant-power setting for the laser diode. The third control input source uses the output from the PD #3 (for LD #1) or PD #4 (for LD #2) TIA to establish a constant-power setting for the laser diode.

Laser Diode Connectors

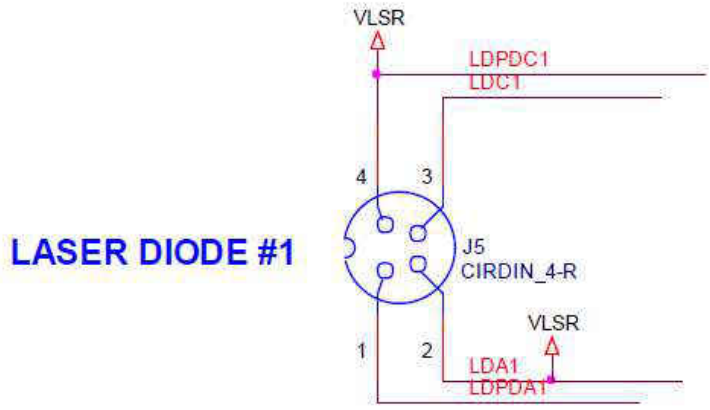

Figure XIII: Laser Connectors

Reference: Translume.Inc.

Pin 1: PD ANODE

Pin 2: LD ANODE (= VLSR)

Pin 3: LD CATHODE

Pin Note that Pin 2 and Pin 4 both connect to VLSR, making 3-lead (LD anode sharing a common pin with the PD cathode) and 4-lead (independent LD and PD anodes and cathodes) function identically from the standpoint of the circuitry on the board. Note also that there is no

ground pin on J4/J5 to accommodate a Case connection. If a Case pin is available it can either be left unconnected, or it can be connected to a signal ground at header connector P4 (see description below). Twenty-six pin header connector P4 also includes connections for both laser diodes (and all four photodiodes), allowing for laser diodes to be placed on a remote board that is then cabled or directly attached to the PDLD Board. Furthermore, P4 includes ground connections that allow an LD Case lead to be connected to Ground. The P4 laser diode connections are as follows:

Pin 17: LD #1 PD CATHODE (= VLSR) Pin 18: LD #2 PD CATHODE (= VLSR)

Pin 19: LD #1 LD ANODE (= VLSR) Pin 20: LD #2 LD ANODE (= VLSR)

Pin 21: LD #1 LD CATHODE Pin 22: LD #2 LD CATHODE

Pin 23: LD #1 PD ANODE Pin 24: LD #2 PD ANODE

Pin 25: Ground Pin 26: Ground

Theory of Operation

Since both of the laser diode circuits are identical, we will describe the operation of the LD #1 circuit here – including specific component reference designators – and the description will apply correspondingly to the LD #2 circuit. 4: PD CATHODE (= VLSR).

LD Control Source Selection:

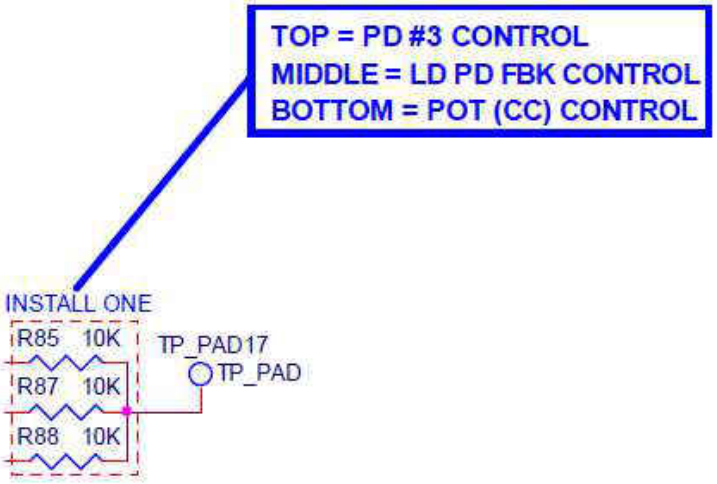

Figure XIIII: LD control Source Selection

Reference: Translume.Inc.

Three resistors – R85, R87 and R88 – are used to select which signal source is to be used for the laser diode control; only one of these 10kΩ resistors should be installed at any given time. If R85 is installed, then independent-feedback constant-power mode is selected, with the signal source being the output of the PD #3 TIA; normally the optional pot (RV2) and its corresponding series resistor (R58) would be used in the PD #3 TIA feedback path to allow for the laser diode power setting to be adjusted. If R87 is installed, then integrated-feedback constant-power mode is selected, with the signal source being the output of the TIA associated with the PD integrated in the laser diode. In this case, pot RV4 would be used to adjust the laser diode power setting. If R88 is installed, then constant-current mode is selected, and the signal source is a voltage divider created by RV5 and R90, with RV5 then being used to adjust the laser diode current setting.

Laser Diode Drive and Feedback:

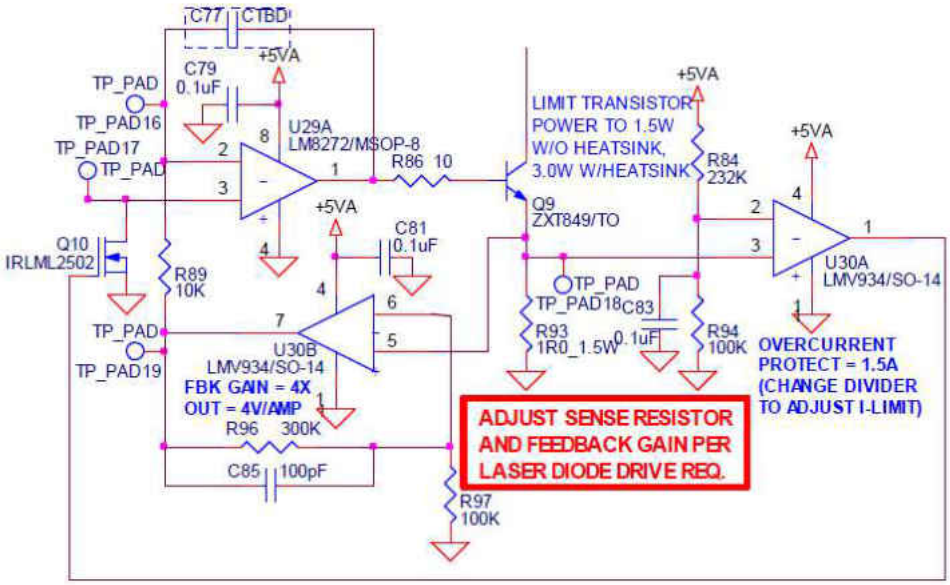

Figure XV: Laser Diode Drive and Feedback

Reference: Translume.Inc.

Transistor Q9 is the laser diode drive transistor. While the schematic shows a base resistor (R86) value of 10Ω, the correct value is 301Ω, 1%. Op amp U29A (LM8272) drives the Q9 base to adjust the (collector) current through the attached laser diode. U29A adjusts the laser diode current until the voltage at the op amp's inverting input (pin 2) – from the current-sense feedback circuit – matches the "demand" or control voltage at the op amp's non-inverting input (pin 3). The control voltage signal source is normally scaled so that 4V represents full scale (maximum laser diode current), but this is not required. While the schematic shows the U29A feedback capacitor (C77) as TBD, a 10nF cap must be installed at this location. The laser diode cathode connects to the collector of Q9. The laser diode anode connects to VLSR. The value of VLSR should normally not exceed about 12V. It is particularly important to avoid excessive power dissipation in Q9, as discussed in detail below. Resistor R93 is the laser diode current-sense resistor. The value of this resistor will vary depending on the approximate diode current

desired. The board is layed out to accommodate a large, 1.5W “2512” size surface-mount resistor for use with high-current laser diodes, or a smaller, ¼W “1206” size resistor for use with low-current laser diodes. It is important to ensure that a resistor with the appropriate power rating is used based on the resistor value and the maximum laser diode current; the minimum resistor power rating is the resistance times the square of the maximum laser diode current. A resistor with 1% or better precision should be used in this location.

The current determined by measuring the voltage across the current-sense resistor (at TPD18) divided by the nominal current-sense resistor value is the laser diode current within ±2%. The voltage across the current-sense resistor is multiplied by the U30B feedback circuit (an LMV934 op amp) before being provided to the inverting input of the control op amp, U29A. The gain (Av) of the feedback circuit is determined by the values of R96 and R97 as determined by the following formula: Av = 1 + R96/R97. The gain is 4.0 in the default configuration, which is reasonable for most implementations. Several parameters and component values must all coordinate to achieve the desired laser diode operation within the limits of the drive circuitry. Specifically, the values of the current-sense resistor, the current sense feedback gain, and VLSR must all work together based on the desired maximum laser diode current. In this section we will discuss how to select the proper component values based on the laser diode characteristics.

The important laser diode parameters to know are:

- Maximum forward current
- Maximum forward voltage
- Minimum forward voltage

Assuming the laser diode control signal source uses 4V to represent full scale (maximum laser diode current) and the gain of the current-sense feedback is at its default value of 4.0, a voltage of 1.0V across the current-sense resistor represents the maximum current through the laser diode. The current-sense resistor should, then, be selected according to: R = 1.0V/(Max LD Current). Thus, for example, to allow for a maximum laser diode current of 40mA, the value of the current sense resistor would be R = 1.0V/0.040A = 25Ω; use the nearest 1% value = 24.9Ω. The maximum laser diode current should not exceed 1.0A. Next, make sure the current-sense resistor has a sufficient power rating. Continuing with our example, the minimum required power rating is 0.0402A * 24.9Ω = 39.8mW, so a standard size 1206, ¼W resistor will work. The next step is to determine the value of VLSR and the maximum power dissipation of the laser drive transistor (Q9). We start be determining the minimum value of VLSR; this is determined by summing the maximum current-sense resistor value (1.0V), plus the maximum laser diode forward voltage, plus the maximum VCE saturation voltage (use 0.2V). So, for example, if the maximum laser diode forward voltage is 2.5V, the minimum value of VLSR is 1.0 + 2.5 + 0.2 = 3.7V. Now we determine the maximum value of VLSR, which is either 12V or the voltage at which we reach the power dissipation limit of the drive transistor. Any increase in the value of VLSR above the minimum voltage previously established is added to the VCE voltage across the drive transistor. In addition, we must assume that the difference between the laser diode's maximum and minimum forward voltages is also added to VCE. The transistor power dissipation is approximately the VCE value times the maximum laser diode current. Continuing with our example, if VLSR is 12V and the minimum laser diode forward voltage is 2.1V, the value of VCE is 12 – 2.1 – 1.0 = 8.9V, and the transistor power dissipation is 8.9V * 0.040A = 356mW. The transistor power dissipation should preferably be kept below 1.0W, although the circuit

board can accommodate up to 1.5W with no heat sink, and up to 3.0W with an appropriate heat sink soldered to the Q9 thermal pad. In general, for low-current (sub-100mA) laser diodes, the Q9 power dissipation is not a concern as long as VLSR does not exceed 12V. For higher-current laser diodes, transistor power dissipation becomes more important and VLSR is preferably kept as close as possible to the minimum allowed value. Note that if it is helpful the circuit can be changed to use a different maximum-current voltage across the current-sense resistor; for example the maximum-current voltage could be 0.5V or 2.0V instead of 1.0V. To adjust for such a change, either the gain of the current-sense feedback circuit would have to change (to 8.0 or 2.0, for example), or the scale of the laser diode control signal would have to change, or some combination of these. For a high-current laser diode example let's assume we have a laser diode with the following

Characteristics:

- Maximum forward current = 850mA
- Maximum forward voltage = 4.0V
- Minimum forward voltage = 3.5V

To select the current-sense resistor we calculate R = 1.0V/0.850A = 1.18Ω (a standard 1% value). The maximum current-sense resistor power dissipation is 0.8502A * 1.18Ω = 0.85W. Since this exceeds the rating of the 1206 size resistor, we select a 1.5W 2512 size 1.18Ω current-sense resistor. We now determined the minimum allowed value of VLSR = 1.0 + 4.0 + 0.2 = 5.2V. We select 6.0V for VLSR. The maximum value of VCE (at maximum laser diode current) is 6.0 – 3.5 – 1.0 = 1.5V. The maximum drive transistor power dissipation, then, is 1.5V * 0.850A = 1.28W. Note that this is higher than the 1.0W preferred limit, but still within the 1.5W capability of the board. Note also that a VLSR value of 6.5V pushes the transistor power

dissipation up to 1.7W, requiring the addition of a heat sink to accommodate the resulting heat. Even if a 6V supply with a 5% output tolerance is used, the maximum 6.3V output voltage results in a transistor power dissipation of 1.53W – slightly exceeding the maximum power allowed without a heat sink. As described in the section Revision A to Revision B Changes, the Rev. B design changed the laser driver amplifier feedback capacitor values from CTBD (undefined) to 10nF, and changed the series output resistors from 10Ω to 301Ω. Both of these changes are incorporated into all Rev. A board assemblies.

Laser Diode Overcurrent Protection:

As shown in the circuit section above, the laser diode driver includes an overcurrent protect circuit, consisting of LMV934 op amp U30A, a pair of resistors (R84 and R94) configured as a voltage divider, and a clamp FET (Q10). The op amp is configured as a comparator, using the output of the voltage divider as a reference. The other input to the comparator is the voltage across the current-sense resistor. The voltage divider output voltage is selected such that it represents the desired overcurrent trip threshold, which is typically 20-50% above the normal maximum laser diode current. Assuming the standard current-sense resistor voltage of 1.0V at the maximum laser diode current, the over current protect voltage divider is normally set between 1.2V and 1.5V (the default). It is important to keep in mind that the trip voltage error is about ±7% after factoring in the +5VA power supply error, the resistor divider error, and the current sense error, so the voltage divider should not be set too close to the normal maximum laser diode current. If the voltage across the current-sense resistor exceeds the voltage divider trip threshold, the output of the U30A comparator goes high, turning on Q10, which clamps the laser diode demand signal to ground, forcing a demand of zero laser diode current. Once the laser diode current drops below the trip threshold, the comparator output will return

low and Q10 will then open, allowing the demand voltage to return to its previous level. Presumably this will again go high enough to trip the overcurrent protect comparator, repeating the cycle. Thus an overcurrent condition will normally result in an oscillation at FET Q10 that results in an effective current limiting through the laser diode. Note that this circuit is designed to protect the laser diode from a catastrophic overcurrent condition that it never expected to occur in normal use.

Constant-Current Control:

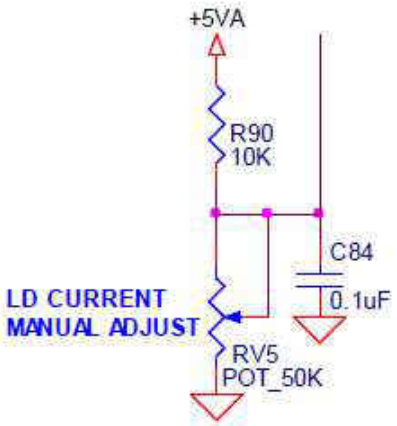

Figure XVI: Constant-Current Control
Reference: Translume.Inc.

For constant-current control mode (R88 installed), pot RV5 is used to adjust to desired LD current. The voltage divider formed by RV5 and R90 establishes a control voltage to the LD drive amplifier (U29A), which can be monitored at TPD17. The voltage divider can range from 0V to about 4V, with 4V representing the maximum LD current. The control voltage to LD current transfer ratio depends on the value of the current-sense resistor and the gain of the current-sense feedback amplifier. Normally the current-sense resistor value is selected to achieve a 1.0V voltage drop at the maximum LD current, which is then multiplied by 4.0 (default) by the feedback amplifier to achieve a voltage that corresponds to the voltage from the RV5/R90 voltage divider.

So, for example, if the current sense resistor (R93) is 25Ω for a 1.0V voltage drop at 40mA, the maximum LD current would be 40mA, and the feedback voltage to the LD drive amplifier would be 4.0V at that LD drive current. The RV5/R90 voltage divider can then be adjusted proportionally to achieve the desired LD current. Using our example, a control voltage of 1.0V would result in an LD current of 10 mA, a control voltage of 2.0V would result in an LD current of 20mA, and so on. Due to component tolerances and the transistor base current that also goes through the current-sense resistor, the actual LD current may vary by as much as ±5% from the expected current based on the control voltage.

Integrated-Feedback Constant-Power Control:

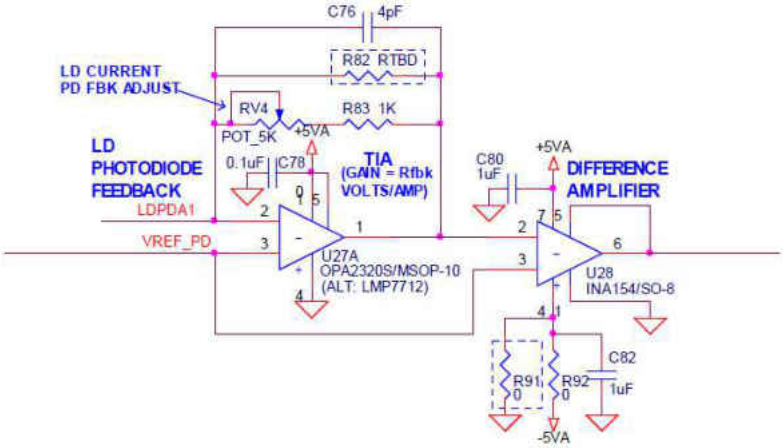

Figure XVII: Integrated-Feedback constant-Power Control

Reference: Translume.Inc.

For LD constant-power operation using the feedback from a photodiode integrated in the same package as the laser diode, a transimpedance amplifier (U27A) is used to convert the photodiode current feedback to a voltage used to control the laser diode current. Resistor R87 must be installed to select this LD control mode. As indicated above, the photodiode cathode will be connected to VLSR, which is the same potential as the laser diode anode. The photodiode anode connects to the input of the TIA. Note that this polarity is opposite that of the TIA's used

in the PD input circuits, which have the photodiode cathode connected to the TIA input. Note that pin 4 of the INA154 difference amplifier connects to -5VA via a 0Ω resistor. There is also a provision for an optional (not normally stuffed) 0Ω resistor to connect pin 4 to AGND instead. The Rev. B design removes the optional resistor to AGND, since the 1µF decoupling capacitor could be replaced with a 0Ω resistor to accomplish the same purpose if needed.

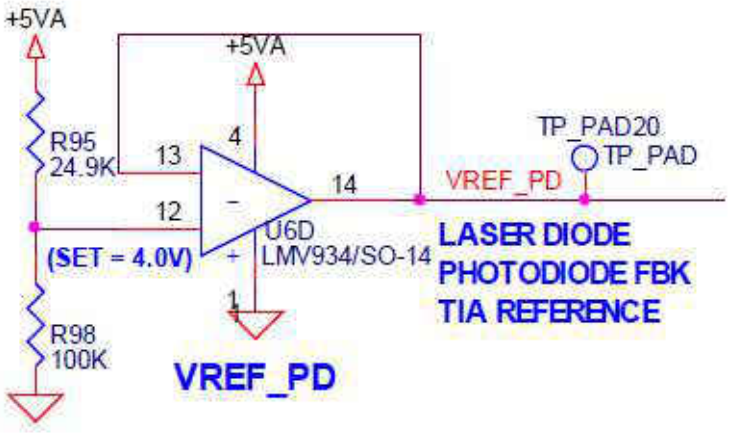

Figure XVIII: VREF_PD

Reference: Translume.Inc.

Because the integrated-feedback TIA is driven by the anode of the integrated photodiode, the TIA output voltage decreases with increased optical power, compared to the TIA's in the PD input circuits which have increasing output voltage with increasing optical power. To accomplish this, the output voltage must be high when no optical power is present. A VREF_PD circuit, shown above, provides a nominal 4.0V reference to the TIA to establish the neutral (no optical power) output voltage, with the TIA output voltage decreasing from there with increasing optical power. It is required that VREF always be higher than VREF_PD, so if VREF is below about 4.5V, VREF_PD should be reduced by adjusting the circuit's voltage divider. The value of VREF_PD can be monitored at TPD20. The gain of the integrated-feedback TIA is established by R83 in series with pot RV4. R83 imposes a minimum gain, while RV4 provides for

adjustability of the feedback to thereby set the desired LD output power. The default values of 1kΩ for R83 and 5kΩ for RV4 permit a TIA gain range of 1000 V/A to 6000 V/A, but other values may be used as needed. Since the TIA output decreases with increased optical power and the LD drive amplifier expects a higher voltage to correspond to increased LD current, it is necessary to flip the polarity of the TIA output; this is handled by the U28 INA154 difference amplifier. This amplifier uses VREF_PD as the reference voltage about which it flips the input voltage from the TIA, creating an output signal to the LD drive amplifier that has the expected polarity.

For integrated-feedback constant-power control, the circuitry on this board is designed to accommodate the following two different LD module choices:

- LD and PD are independent (no connections in common)
- LD anode is internally connected to the PD cathode

Independent-Feedback Constant-Power Control:

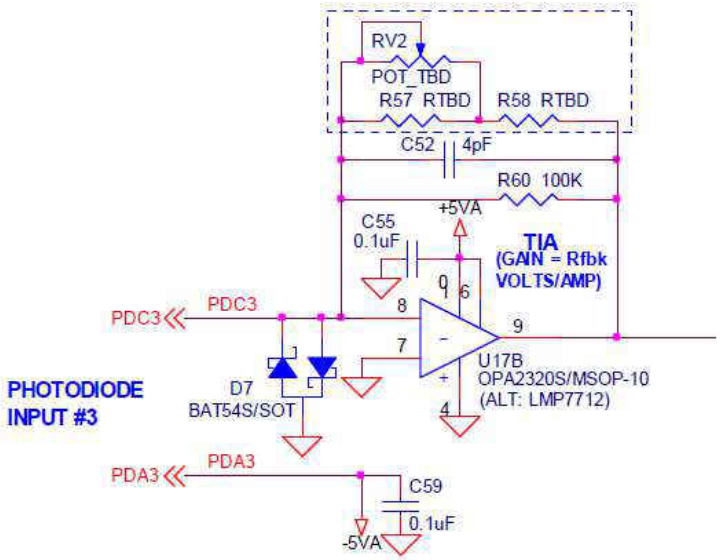

Figure XVIIII: Independent-Feedback Constant-Power Control

Reference: Translume.Inc.

For LD constant-power operation using the feedback from one of the PD input circuits – referred to here as independent-feedback constant-power control – resistor R85 must be installed. In this mode, the LD #1 circuit connects directly to the output of the PD #3 TIA, while the LD #2 circuit connects directly to the output of the PD #4 TIA. The basic operation of the PD TIA circuit was discussed earlier, but it should be noted that if a PD TIA is to be used for LD constant-power control, the "alternate" TIA feedback – consisting of a pot and a series resistor – should be used instead of the single resistor feedback, to allow for adjusting the desired LD output power. The TIA feedback pot/resistor values (representing the TIA gain) must be selected based on the photodiode characteristics and the LD circuit operation, with 4.0V normally representing the maximum LD output power.

REFERENCES

1. Striebich, R. C., et al. (2014). "Characterization of the F-76 diesel and Jet-A aviation fuel hydrocarbon degradation profiles of Pseudomonas aeruginosa and Marinobacter hydrocarbonoclasticus." International Biodeterioration & Biodegradation 93(0): 33-43.
2. Stamper, D. M., et al. (2012). "Depletion of Lubricity Improvers from Hydrotreated Renewable and Ultralow-Sulfur Petroleum Diesels by Marine Microbiota." Energy & Fuels 26(11): 6854-6862.
3. "Optical Nano and Micro Actuator Technology" George K. Knopf, Yukitoshi Otani. Pg-471-489
4. Itah, A. Y., et al. (2009). "Biodegradation of international jet A-1 aviation fuel by microorganisms isolated from aircraft tank and joint hydrant storage systems." Bull Environ Contam Toxicol 83(3): 318-327.
5. Gunasekera, T. S., et al. (2013). "Transcriptional profiling suggests that multiple metabolic adaptations are required for effective proliferation of Pseudomonas aeruginosa in jet fuel." Environ Sci Technol 47(23): 13449-13458.
6. J. E. Sheridan.,et al.(1971)." Studies on the 'Kerosene Fungus' Cladosporium Resinae (Lindau) De Vries Part I. The Problem of Microbial Contamination of Aviation Fuels." Journal of the Biological Society Tuatara: Volume 19, Issue 1, November 1971
7. Cofone, L., Jr., et al. (1973). "Utilization of hydrocarbons by Cladosporium resinae." J Gen Microbiol 76(1): 243-246.
8. The Microflow cytometer."Frances S.ligler, Jason S.Kim. Pg(287-309)

9. Dr. John Choma., “Electronic Noise Characterization − Part I: System Concepts and Theory.” Technical Report #02-0511_R1
10. www.zricoa.com
11. Ph. Bado, A. A. Said, M. Dugan, T. Sosnowski and S. Wright, Dramatic improvements in waveguide manufacturing with femtosecond lasers. Proceedings of the 18th annual National Fiber Optic Engineers Conference (NFOEC 2002), Dallas (TX), 1153-1158 (2002).
12. J. W. Chan, T. Huser, S. Risbudand and D. M. Krol, Structural changes in fused silica after exposure to focused femtosecond laser pulses. Opt. Left. 26, 1726-1728 (2001).

ABSTRACT

FABRICATION AND CHARACTERIZATION OF A ROBUST, FIELD-DEPLOYABLE, OPTICAL SENSOR DESIGNED TO DETECT PARTICLES IN OILS.

by

NAVYA PANDREKA

May 2015

Advisor: Dr. Gregory Auner

Major: Biomedical Engineering

Degree: Master of Science

Some types of bacteria and fungus can use iron or non-ferrous metals for their metabolic process. Sulfate-reducing bacteria can corrode pipes in the oil industry and high-end machinery. Both aerobic and anaerobic bacteria often degrade fuel quality and cause fuel system corrosion or alter the chemical properties of the fluid. This causes significant economic damage and safety concerns. Therefore, there is a need for a system to continuously monitor fuel or lubricant oil for the presence of bacteria and fungus.

The main goal of this project was to develop a sensor that can detect bacteria and other ferrous and non-ferrous debris that are present in the lubricant of high-end machinery in real-time. Utilizing optical techniques to detect and size these particulates. This sensor features a robust optical system paired with microfluidics. When fluid passes within a sampling channel, the particles in the fluid block the laser that is passing through the channel. This laser blockage was detected by a photodetector, creating a microfluidic micro counter.

A novel chip fabrication approach was used with fused silica (a high-quality SiO2 glass). Its material characteristics were locally modified using femtosecond laser pulses to (a) change the fused silica index of refraction, and (b) change its susceptibility to HF etching. The index of refraction change is used to create optical waveguides within the fused silica substrate (this process is called as femtoWriteTM), and the second process (femtoEtchTM) was used to shape the fused silica. This phenomenon occurs due to the ultrashort light pulse whose wavefront has little absorption until deep within the fused silica substrate. The damage or defects created beneath the surface render that portion of the fused silica susceptible to rapid etching by HF.

The efficacy of the chip was shown by spiking 1) ceramic microparticles, 2) Pseudomonas aeruginosa bacteria which causes alkylaromatic degradation, in 5W30 motor oil. These two proofs-of-concept represent two key types of particles which must be monitored in hydrocarbons and fuel systems.

Each of the above particles and biologicals were successfully detected from a 3ml of the oil sample. Ceramic beads, of 100μm size, were used with a concentration 100mg /3ml of oil. The spike voltage and intensity was strong when a bead was passing through the light source with a flowrate of 3ml/min. The spike was dropped from 4.55V to 2.79V with a greater significance of detection in 0.01 seconds. In this case, Pseudomonas aeruginosa bacteria showed less intensity comparing with beads with a voltage drop from 3.469V to 3.441V in 0.02 seconds.

AUTOBIOGRAPHICAL STATEMENT

EDUCATION

Graduate Education (MS)

Master of Science Biomedical Engineering, Wayne State University, Department of Biomedical Engineering, College of Engineering: Dr. Gregory Auner

Undergraduate Education (B. Tech)

Bachelors of Technology Biotechnology, Gokaraju Rangaraju Institute of Engineering and Technology, India.